UNIVERSITÀ DEGLI STUDI DI PADOVA

Dipartimento di Fisica e Astronomia "Galileo Galilei"

Corso di Laurea Magistrale in Fisica

Tesi di Laurea

Perspectives on the measurement of competitive double gamma decay with the AGATA tracking array

Relatori
Dott. Jose Javier Valiente Dobón
Dott. Alain Goasduff

Laureando
Daniele Brugnara

Anno Accademico 2017/2018

Daniele Brugnara: *Perspectives on the measurement of competitive double gamma decay with the AGATA tracking array ,* subtitle, © September 2018

ABSTRACT

This thesis is a feasibility study of the competitive double-gamma decay measurement with the AGATA gamma-ray tracking array. This process consists in the decay of an excited nuclear state to another via emission of two prompt gammas, even when the emission of a single photon is possible and is generally characterized by low branching ratios ($10^{-6} - 10^{-8}$). A simulation study as well as a first approach to experimental data are discussed, in order to test different aspects of this experimentally challenging measurement. Particular emphasis is placed in the tracking algorithm which allows to reconstruct a scattering event based on the position and energy of every interaction point within the AGATA germanium detector.

CONTENTS

Part I

SCIENTIFIC INTERESTS OF THE DOUBLE-GAMMA DECAY PROCESS AND THE EXPERIMENTAL APPARATUS

This first section serves as an introduction to the various concepts that will be discussed in the course of the thesis. The scientific interest of this decay process within nuclear structure and more in general nuclear physics will be motivated. Emphasis will be put on why the versatility of the AGATA tracking array makes it a good candidate for future challenging measurements of this decay process.

1 INTRODUCTION

The double-gamma decay is an electromagnetic process where two photons are emitted simultaneously. It can occur between states where a single photon transition is prohibited due to spin conservation (namely in a $0^+ \to 0^+$ transitions) as well as in competition with the single gamma emission or other nuclear decay processes.

The theory behind the decay [1] is well described by the perturbative QED formalism, together with the knowledge of the nuclear structure of the decaying nucleus. Feynman diagrams are thus introduced, while the nuclear matter is treated non-relativistically. The concept of virtual particle or propagator, which is crucial in the quantum field theory reasoning, is thus substituted by the idea of virtual nuclear state. The heuristic interpretation of a virtual particle or nuclear state (Figure 1) is that, if short enough for the uncertainty principle, a quantum state can temporarily violate the conservation laws thus permitting the development of the process. In the figure, in red, is shown the transition through one virtual higher energy nuclear state; the width of the decay is found by summing over all possible virtual states.

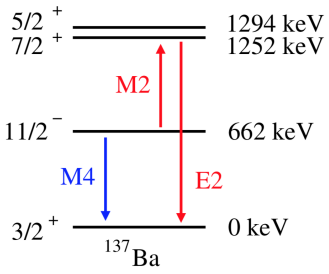

Figure 1: Decay scheme for the emission of a single photon (blue) and a double-gamma via the transition in the virtual nuclear state.

This decay channel was first observed 1959 and the following decades. First measurements were limited to setting an upper limit on the branching ratios, while successful observations were later carried out with ^{16}O, ^{40}Ca and ^{90}Zr [2] between the ground state and the first excited nuclear state ($0^+ \to 0^+$). Due to the conservation of the total angular momentum, a pure gamma transition is not possible. In the case of ^{16}O, for instance, with a branching ratio of $\Gamma_{\gamma\gamma}/\Gamma_{tot} = (6.6 \pm 0.5)\,10^{-4}$, the state can decay via simultaneous E1-M1 multipolarity transitions.

A recent article [3] was published on Nature regarding a first observation of this process for transitions where the single-gamma decay is allowed, namely in the case of ^{137}Ba between the $\frac{11}{2}^-$ and $\frac{3}{2}^+$ states, with $\Gamma_{\gamma\gamma}/\Gamma_{\gamma} = (2.05 \pm 0.37)\,10^{-6}$. The measurement took place at TU Darmstadt and made use of an array of $LaBr_3$ scintillators, taking advantage of the good timing properties of these detectors to distinguish real events from a background composed by natural radiation and photons scattering between nearby detectors.

While some attempts of measuring this process with High Purity Germanium (HPGe) detectors have been carried out [4], none of them resulted in a positive outcome.

The thesis will mainly focus on the perspectives and challenges of the measurement with the state-of-the-art gamma spectrometer AGATA. The intent is to quantify, in a first test of the problem with this particular setup, if its ability to reconstruct scattering gamma-rays will be able to overcome the various challenges that this measurement poses. A detailed simulation of the response of the array to single and double-gamma emissions in ^{137}Ba will be proposed. The intent of such a decision is to asses the problem in the arguably simplest case scenario, thus serving as a first test of feasibility of the measurement. While this decay channel can occur in any gamma nuclear transition, the branching ratio can vary widely and, in general, is more important for higher multipolarity transitions, which are characterized by lower transition probabilities.

1.1 SCIENTIFIC MOTIVATIONS

From an experimental standpoint, the interests behind the measurement are multiple. In the search of the future of gamma spectroscopy, the scientific community needs to determine the capabilities and limits of the current experimental apparatuses in order to understand where it is necessary to invest research effort and funds. In fact, as every field of research is characterized by the ever lasting quest for its future scopes, knowing the potential and limits of the available setups is crucial for the progress of the scientific knowledge.

From a theoretic point of view, a nuclear model can be thought as a mathematical and physical tool to explain observed phenomena as well as predict what has not been yet observed. While a model often needs some experimental input, its success is also tested on its ability to reproduce what is measured. Having more observables means being able to further put the model to the test. In fact, the decay width and thus the branching ratio, as hinted in Section 1.2, depends on off-diagonal matrix elements which allows to characterize nuclear properties such as electric polarizabilities and magnetic susceptibilities. Different observables might be sensible to different aspects of nuclear wave-functions and a complete set of measurable quantities is the key to understand the properties of the nuclear matter and its interactions.

At last, the quest for the detection of neutrino-less double-beta decay is one of major open question in contemporary physics. This decay process is considered one of the most promising to observe lepton-number violation experimentally and its observation would prove that neutrinos are their own antiparticles. The lifetime of the decaying state depends on the nuclear matrix element, which is sensitive to the nuclear structure of the parent and daughter nuclei. A reliable calculation of these quantities has not been agreed on as many models are in disagreement, limiting the full understanding of the experimental reach in the topic [5]. Recent theoretic developments, which are still under investigation [6], point towards a similarity between matrix elements relative to this very process and those of the double-gamma decay, making its study a very compelling topic.

1.2 DOUBLE-GAMMA DECAY: THE PHYSICAL PROCESS

The theory behind this decay process has been studied extensively in 1960 by D. P. Grechukhin ([7] and previous works) and a more complete formulation has been given by J. L. Friar [8] and by the authors of the first double-gamma decay observation with ^{16}O [1].

The combination of the quantum field theory treatment with non relativistic nuclear matter has been proved in good agreement with the experimental results even in the competitive double gamma case [3].

Up to the second perturbative order, which coincides with the emission of two photons, three diagrams contribute to the process:

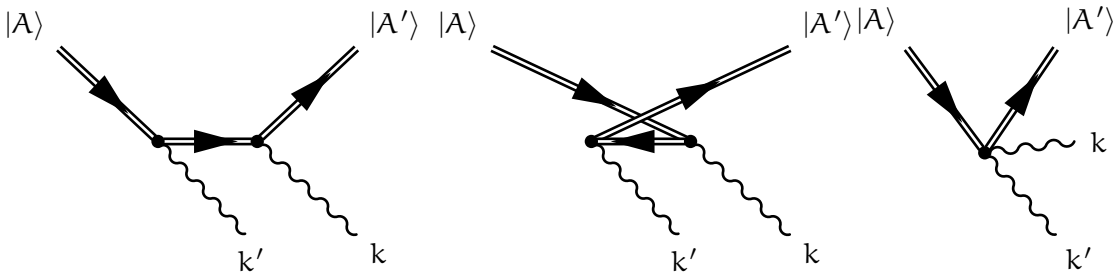

The final Feynman amplitude consists in the interference of the three diagrams, where the rightmost is introduced as a correction to the non relativistic treatment of the nuclear Hamiltonian, and is usually referred to as the Seagull amplitude.

In the Dirac notation, the quantum initial and final states are labeled as:

$$\begin{cases} |F\rangle = |\alpha' I', M', P'\rangle \otimes |k, \lambda\rangle \otimes |k', \lambda'\rangle \\ |I\rangle = |\alpha I, M, P\rangle \end{cases}$$

	α	Nuclear structure quantum numbers
	I and M	Initial total nuclear angular momentum numbers
Where	I' and M'	Final total nuclear angular momentum numbers
	P	Single particle momentum
	k, k' and λ, λ'	Photon wavenumbers and helicities

The Hamiltonian of the process consists in the nuclear matter current j_μ coupled to the electromagnetic field A^μ and with the the seagull correction term $B_{\mu\nu}$ coupled with two electromagnetic fields:

$$\mathcal{H}_{int} = \underbrace{\int d^3\mathbf{x}\, j_\mu(x) A^\mu(x)}_{\mathcal{H}_1} + \underbrace{\frac{1}{2}\int d^3\mathbf{x}\, d^3\mathbf{y}\, A^\mu(x) A^\nu(y) B_{\mu\nu}(x,y)}_{\mathcal{H}_2}$$

Developing the time ordered product of the couplings, a second order process is characterized by a "nuclear matter propagator" between two quadri-positions $\mathbf{x}$ and $\mathbf{y}$ for the first diagrams, while the remaining diagram is in itself a second order perturbation.

Thus the Feynman amplitude of the process takes the following form

$$M_{fi} = -\frac{ie^2}{\sqrt{4\omega\omega'}}\epsilon^{\mu}(k,\lambda)\epsilon^{\nu}(k',\lambda')\int d^3\mathbf{x}d^3\mathbf{y}e^{ik\cdot x+ik'\cdot y}\,\langle \alpha\, I, M, P|\,(T\,[B_{\mu\nu}(x,y)] - iT\,[J_{\mu}(x)J_{\nu}(y)])\,|\alpha'\, I', M', P'\rangle$$

Which is used to compute the final partial differential decay width of the state, which includes the phase spaces as well as the quadrimomentum conserving Dirac delta:

$$d^9\Gamma = (2\pi)^4\delta^4(P_f - P_i + k + k')\sum_f\left(\frac{d^3\mathbf{P_f}}{(2\pi)^3}\right)\left(\frac{d^3\mathbf{k}}{(2\pi)^3}\right)\left(\frac{d^3\mathbf{k}'}{(2\pi)^3}\right)\frac{(2\pi)^2}{4\omega\omega'}\left|\bar{M}_{fi}\right|^2$$

The differential width is of the ninth order due to the three particle final state, however the Dirac delta fixes 4 degrees of freedom, thus resulting in a 5 *d.o.f* differential width ($d^5\Gamma/d\omega d\Omega d\Omega'$). The development of the calculation involves switching to the Landau gauge in the multipole expansion and rotating the quantization axis in a reference system where it is parallel to the photon wave-vector with the rotation matrices $D^L_M(\theta,\phi)$. The Feynman amplitude obtained has the following form [1]:

$$M_{fi} = (-1)^{I_f - M_i}\sum_{LL'JMM'SS'}(2J+1)(-1)^{L+L'}\begin{Bmatrix} I_f & J & I_i \\ -M_f & m & M_i\end{Bmatrix}\begin{Bmatrix} L & L' & J \\ M & M' & -m\end{Bmatrix}\lambda^S\lambda^{S'}P_J(ML, M'L', \omega\omega')D^L_{M-\lambda}(\theta,\phi)D^{L'}_{M-\lambda'}(\theta',\phi')$$

The result is a transition amplitude which depends on the sum over all virtual states matrix elements, namely the so called *generalized polarizabilities* $P = P^{res} + P^{sg}$. The first two diagrams contribute to the polarizabilities with P^{res}:

$$P^{res}_J(S'L'SL, \omega\omega') = 2\pi(-1)^{i_i+I_f}\sqrt{2L+1}\sqrt{2L'+1}\sum_n\left(\begin{Bmatrix} L' & L & J \\ I_i & I_f & I_n\end{Bmatrix}\frac{\langle I_f\|O(S',L',\omega')\|I_n\rangle\langle I_n\|O(S,L,\omega)\|I_i\rangle}{E_n - E_i + \omega} + (-1)^{L'+L+J}\begin{Bmatrix} L' & L & J \\ I_i & I_f & I_n\end{Bmatrix}\frac{\langle I_f\|O(S,L,\omega)\|I_n\rangle\langle I_n\|O(S',L',\omega')\|I_i\rangle}{E_n - E_i + \omega'}\right)$$

And for the seagull amplitude:

$$P^{sg}_J(ML, M'L', \omega\omega') = -\sqrt{\pi}\frac{(2L+1)^{3/2}(2L'+1)^{3/2}}{\sqrt{2L+1}}\begin{Bmatrix} L' & L & J \\ 0 & 0 & 0\end{Bmatrix}\begin{Bmatrix} L' & L & J \\ L' & L & 1\end{Bmatrix}\frac{\omega'^{L'}}{(2L'+1)!!}\frac{\omega^L}{(2L+1)!!}\langle I_f\|\frac{i^{L'+L}}{m}\sum_J e_J^2|\mathbf{r}_J|^{L+L'}Y_j(\hat{\mathbf{r}}_J)\|I_i\rangle$$

These expressions depend on the off-diagonal matrix element relative to the magnetic and electric multipole operators in the long wavelength approximation (due to the Bessel functions expansion):

$$O(EL,\omega) = \sqrt{\frac{L+1}{L}}\frac{i^L\omega^L}{(2L+1)!!}\underbrace{\int d^3\mathbf{x}\,\rho(\mathbf{x})|\mathbf{x}|^L Y_{LM}(\hat{\mathbf{x}})}_{M(EL,M)}$$

$$O(ML,\omega) = \sqrt{\frac{L+1}{L}}\frac{i^{L-1}\omega^L}{(2L+1)!!}\underbrace{\int d^3\mathbf{x}\,\mathbf{j}(\mathbf{x})(\mathbf{x}\times\nabla)|\mathbf{x}|^L Y_{LM}(\hat{\mathbf{x}})}_{M(ML,M)}$$

The generalized polarizabilities need to follow the common selection rules on parity and angular momentum conservation:

$$\begin{aligned}(-1)^{L+S+L'+S'} &= \pi_i\pi_f\\ |I_i - I_f| \leqslant J &\leqslant |I_i - I_f|\\ |L - L'| \leqslant J &\leqslant |L + L'|\end{aligned}$$

In the case of ^{137}Ba, a good approximation is to consider only the lowest spin transition $J = 4$ and a single particle nuclear model. This isotope is one neutron away from the shell closure of $N = 82$, and in first approximations, all protons are coupled in pairs and can be neglected. As a consequence, the nuclear levels can be considered as neutron hole excitation to the higher lying states. If only the main contributions to the width are taken into account (M2-E2 and M1-E3 multipolarities), it is possible to obtain $\Gamma_\gamma/\Gamma_{\gamma\gamma} = 2.06\times10^{-6}$ [9]. A more complete model (QPM, quasi-particle phonon model) [3], returns a ratio between decay widths of $\Gamma_\gamma/\Gamma_{\gamma\gamma} = 2.69\times10^{-6}$.

1.3 GAMMA INTERACTION WITH MATTER

A gamma-ray spectroscopy experiment relies on the ability to fully absorb the incident photon in the detector in order to measure its energy with the highest possible precision. A high interaction cross section is thus crucial in this field of study.

Specifically, to fully deposit its energy, the photon has to interact via photoelectric effect [10], as a Compton scattering interaction, for instance, only allows for a partial deposition of energy. As a consequence, maximizing the cross section of the former will improve the results in the measured spectrum.

Germanium detectors have found their use in high resolution gamma-ray spectroscopy thanks to their high atomic number which allows for high photoelectric cross sections as well as good semiconductor properties resulting in good energy resolution (if properly cooled at liquid nitrogen temperatures).

In the detection of gamma rays, the study of their interactions with matter is necessary. In general there are four types of interaction:

- *Rayleigh scattering*: the photon is elastically scattered, changing direction but keeping unchanged energy. Due to these reasons, this process could be a

challenge for a tracking array, however its low cross section in the energies of interest, compared with the other interaction mechanisms greatly reduces the problem.

- *Photoelectric absorption*: the photon is absorbed by a shell electron which passes in the conduction band, producing a signal proportional to the energy of the incident gamma minus the electron shell binding energy. This process is dominant for energies below 200 keV.
- *Compton scattering*: the photon is scattered depositing some of the energy in the electron it has interacted with. A kinematic condition relates the scattering angle with the energy of the scattered gamma ray:

$$E' = \frac{E_0}{1 + \frac{E_0}{m_e c^2}(1 - \cos\Theta)} \tag{1}$$

- *Pair production*: a photon passing through matter has the possibility of interacting with a non quantized field producing a particle-anti particle pair, namely electron and positron in the range of energies of nuclear physics. This process has a threshold of two times the mass of the electron and mainly occurs at energies above 7 MeV.

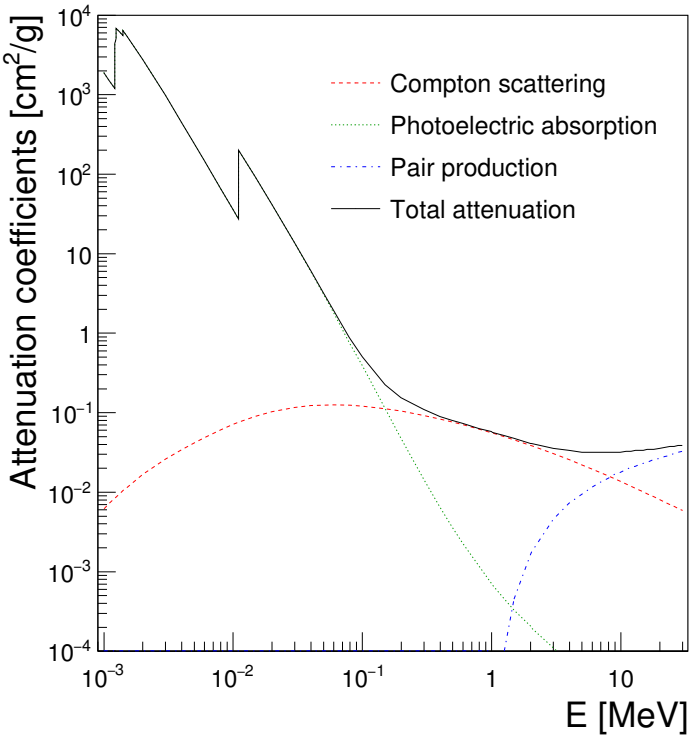

s

Figure 2: Interaction cross section of a gamma ray with Ge. Photoelectric effect dominates the interaction at low energies while pair production is mostly relevant at high energies. Compton interaction is prominent in the range or energy of interest in nuclear physics. Figure adapted from [11].

The cross section σ can be defined as the proportionality constant which binds the change of particle flux as a function of the material thickness:

$$\frac{d\Phi}{dz} = -n\sigma\Phi \quad \Longrightarrow \quad \Phi = \Phi_0 e^{-n\sigma z}$$

Where n is the numeric density of scattering centers and z the material thickness. The number of particles passing through matter decays exponentially with z. The cross section itself is a function of many parameters, notably, in the case of a photon, the energy of the incident gamma ray and the properties of the material.

In the case of Germanium the attenuation cross sections as a function of the energy is shown in Figure 2 with contributions from the various processes broken down.

In gamma spectroscopy, the ideal detector would have high P/T ratio, high efficiency and energy resolution. While the perfect detector does not exist, to maximize the photoelectric absorption process, a high number of electrons (high Z) is needed, as the photoelectric cross section is proportional to $\sigma_{ph} \propto Z^x$ with $x \in [4, 5]$.

1.4 THE EXPERIMENTAL CHALLENGE

As discussed in reference [3], one of the most pressing experimental challenges in the observation of the competitive double-gamma decay arises from its branching ratio, which is more than five orders of magnitude smaller than that of the main transition channel. In an ensemble of nuclei undergoing gamma decay from a given excited state, a large number of gamma quanta are emitted, which generates two fundamental challenges:

1. a photon with energy E_0 can deposit part of its energy E_1 in one detector of the array and scatter to another one where E_2 is measured. If the photon is fully absorbed, $E_1 + E_2 = E_0$. This type of event is very common in the range of energies of interest, as shown in Section 1.3. Since the sum of the energies registered in both detectors equals the transition energy, it presents the same signature of the (competitive) double-gamma decay (Figure 3).

2. two gamma quanta, can be emitted independently by two nuclei with a time difference too small to be discriminated and deposit a fraction of their energy in two detectors, such that the energy sum is again close to E_0. Although these random coincidences can be subtracted from truly simultaneous events, they cause a substantial statistical uncertainty, thereby preventing the observation of the much rarer competitive double-gamma decay unless an effective suppression method is found.

Due to these problematics, various arrays have different methods to suppress these events. Fast scintillators like $LaBr_3$ (used in reference [3]) have a time resolution which can range between 100 ps to 1 ns, depending on their size, allowing to discriminate prompt and scattered events based on their time difference.

High purity germanium detectors, on the other hand, do not have this capability due to a lower timing resolution (in the order of 10 ns). In fact, a quick calculation

returns that in this resolving time, a photon has traveled about 3 m, a length much higher than the dimensions of a typical HPGe array.

However, other powerful methods have been or will be attempted, such as Compton shields (GAMMASPHERE, [4]) or the fact that the angle of scattering and the energy of the scattered photon are binded by equation 1.

If it is possible to detect both the angle of scattering θ and the scattered energy E', it is also possible to discriminate the first type of events from the second, as multiplicity two gammas do not have the same restrictions.

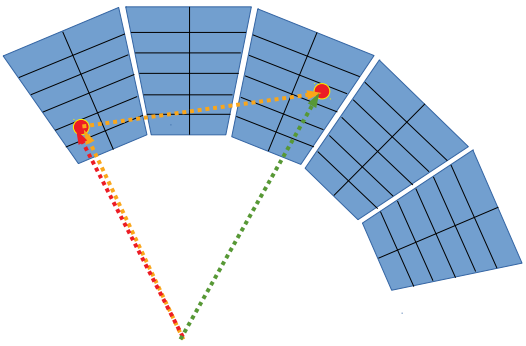

Figure 3: Representation of a single gamma-ray (in yellow) scattering inside an array of detectors. In green and red the emission of two simultaneous photons.

AGATA, the array tested in this thesis has this exact capability: to measure the position of interaction of the photon thanks to a segmentation of the Germanium crystals. As a consequence, what needs to be understood is weather the precision of a discrimination based on this property will be enough to operate a selection as effective as the one used in reference [3].

In fact, thanks to its high energy resolution, angle resolving capabilities and higher efficiencies, the AGATA array would be an excellent candidate for the measurement of the competitive double-gamma decay. If capable, the array would open the possibility of numerous observations of this very process in other nuclei.

1.5 AGATA: THE ADVANCED GAMMA TRACKING ARRAY

The array [12] is the state-of-the-art gamma-ray spectrometer, combining the high energy resolution of HPGe detectors with high efficiency and angular resolution.

The idea behind the setup is to make use of multiple segmented HPGe crystals in order to detect not only the energies of the gamma interactions within the array, but also their positions. This allows for the reconstruction of the path taken by the gamma ray, as will be discussed more in detail in the following sections. The ability to reconstruct scattering photons makes the use of Compton shields [10] unnecessary, so that higher solid angle coverage can be taken up by HPGe detectors, ultimately leading to higher efficiencies.

This gives the setup an unprecedented versatility, crucial feature for the scope of the measurement considered in this thesis.

The array, in its current state consists in 35 detectors with 36 segments each and a common central core, as shown in Figure 4. The long term project plans to cover the 4π solid angle with a total of 180 crystals, which would allow for an unprecedented photopeak efficiency of $\approx 43\%$ at 1MeV for multiplicity 1 photons (3% resolution) and an even more astonishing efficiency of $\approx 28\%$ for multiplicity 30 gammas at the same energy [12].

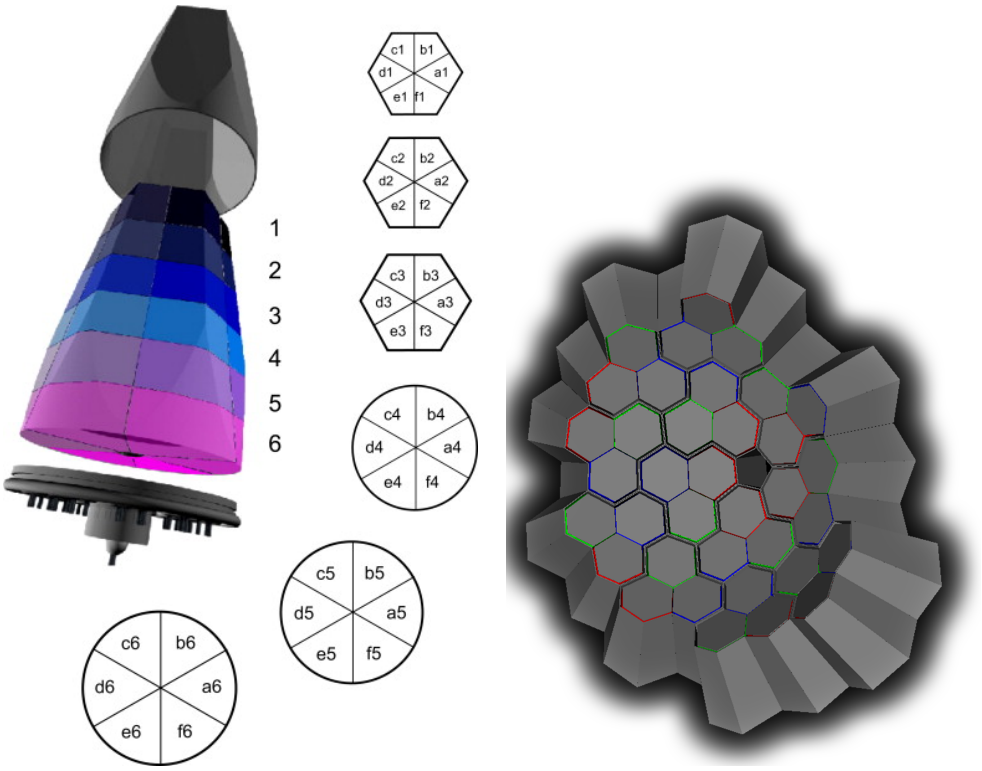

(a) (b)

Figure 4: (a) Render of the segmented crystal with the cross section in various depths. (b) Render of the current crystal configuration as simulated with the AGATA simulation code [13] as well as current experimental setup. The pentagonal hole is present for the beam line, as the array is currently located at back scattering angles with respect to the target.

The AGATA detectors consist in *n-type* high purity germanium (HPGe) crystals with tapered hexagonal shapes and, when properly arranged, form a 90 mm thick segmented Germanium shell, with 235 mm inner radius. Each crystal is enclosed in a vacuum sealed aluminum canister of 0.8 mm thickness. The segmented hexagonal HPGe crystals (Figure 4 (a)) are grouped in triple clusters [14] which have a common refrigerating liquid nitrogen dewar. Each of the three crystal in the cluster has a color assigned (R, G or B), and is polarized by a HV tension of up to 5000 V via the core electrode.

The specified FWHM at 1.33 MeV is lower or equal to 2.35 keV ($\approx$ 1.8% resolution) for the core and 2.3 keV for the segment. The nominal position resolution depends strongly on the energy of the incident gamma [15], and its reference value is set at around $4-5$ mm. In practice, both quantities depend on the state of the crystal, namely how much neutron damage is affecting the detector, as will be observed in Chapter 3, sections 3.2.3 and 3.2.1.

The basic data acquisition of such a complex array can simplistically synthesized in eight main steps [12]:

1. The segmented HPGe crystals produce various electric signals after the interaction of a gamma ray. The segment signal is sent to individual low noise preamplifiers.

2. The output is sent to the digitizers where a trigger is applied on the core signals and, when activated, acquires the signal of all 36 segments.

3. The traces are converted into digital format by custom digitizers which transfer the produced data to the pre-processing electronics.

4. The pre-processed data is sent to a server where a pre-PSA filter (Pulse Shape Analysis) is applied and a first calibration is performed. The traces are analyzed by the chosen PSA algorithm [16] and the interaction position and energy deposited are computed.

5. Once the position is obtained by the PSA filter, a neutron damage algorithm is applied to correct for the loss in the collected charge and to recover the best possible energy resolution.

6. An event builder merges the data of all the crystals and creates events, intended as sets of interaction points within a chosen time interval.

7. Built events are merged with ancillary detectors, if present.

8. The merged events are tracked by the algorithm of choice, in order to reconstruct the path of the gammas using the interaction points, thus reducing the Compton distribution generated by photons scattering on the Germanium crystals.

While a more complete description of the electronics as well as other experimental aspects are presented in reference [12], an introductory discussion on the PSA and the tracking algorithm is hereby proposed.

1.5.1 *PSA: Pulse Shape Analysis*

When a gamma ray interacts with the detector, a pulse of current is registered in the inversely polarized semiconductor. The shape of the pulse can be studied to determine the position of the interaction due to many reasons [17, 18], some of these aspects include:

- The difference in drift velocity between holes and electrons makes the signal dependent on the distance of the interaction from the core central contact, as depicted in Figure 5 (top).

- The anisotropy of the drift velocity in the crystalline structure of the semiconductor (dependent on the crystal plane) generates a variation of the pulse on the ϕ angle of the detector.

- Mirror charges are also generated in segments nearby the one that has been hit (Figure 5 (bottom)). These shapes can also be analyzed and are dependent on the interaction position.

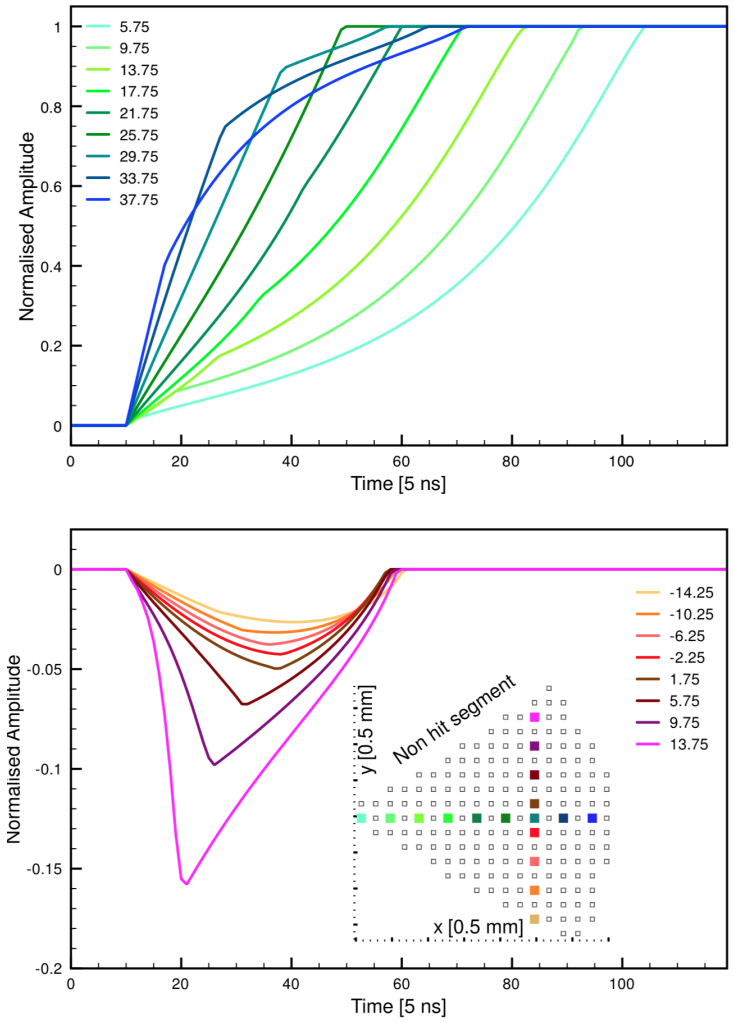

Figure 5: Simulated signals in an AGATA detector: (top) Central contact signal for several interaction radii. (bottom) Induced signal in a not-hit segment (transient signal) depending on the position interaction in the hit segment. The insert in the bottom panel indicates the relative position interaction position. The difference in drift velocity between holes and electrons as well as the drift velocity dependence on the crystalline plane differentiate the measured signals (Figure adapted from [19]).

While the shape determines the position, the total collected charge is proportional to the deposited energy; the determination of the proportionality coefficient is referred to as the calibration of a detector. In AGATA the calibration process is performed multiple times at various levels of the data acquisition system.

1.5.2 *Tracking algorithm*

The tracking is the main focus of this work as the ability to reconstruct an event is, as will be argued, one of the main limiting factors in the measurement of the competitive double-gamma decay. This process, due to its low-branching ratio, requires a precise reconstruction of every event, namely it needs to be able to not

only track correctly a double-gamma event but also to avoid errors in reconstructing single photons. There are multiple algorithms developed to carry out this task in AGATA, the performance of each has been thoroughly tested and compared [20]. The most commonly used algorithm is called forward tracking, of which two versions exist: MGT [21] and OFT (Orsay Forward Tracking) [20].

The OFT algorithm consists in assigning to a path, a ordered set of interaction points, a merit factor which is related to the probability that the gamma ray has scattered accordingly and thus deposited the measured energy as registered by the hit segments.

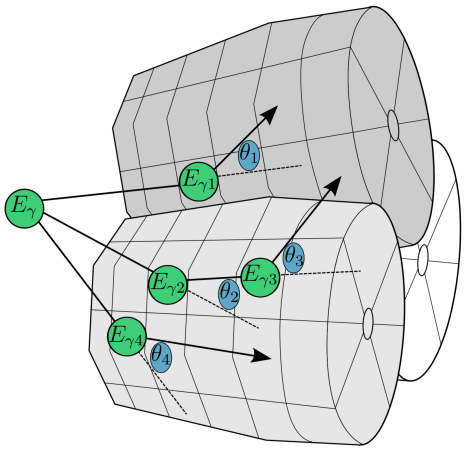

Figure 6: Schematic representation of gamma rays emitted from a source and interacting by Compton effect in one of AGATA's triple clusters (adapted from [22]). The angle of scattering and the deposited energy $E_{\gamma i}$ are related by equation 1.

The first step taken by the tracking algorithm is called clustering. Groups of interaction points, clusters, are created by progressively incrementing the aperture from a minimum angle and grouping points with angle inferior to it. The maximum aperture angle search is a function of the number of interaction points. While this feature is important in an in-beam experiment, the maximum angle was set to 2π in the course of the simulation, to test all possible configurations of clusters.

Each cluster is then assigned a merit factor which consists in the product of various terms that are related to:

- The probability of the gamma ray to pass through a given distance of germanium.
- The photoelectric absorption cross section if the interaction point is considered the last hit.
- The likelihood of a Compton event, based on the kinematic relation of electron-photon scattering:

$$\exp\left(-\frac{(E_{geom}-E_m)^2}{\sigma^2}\right) \tag{2}$$

where E_m is the measured energy, E_{geom} is the energy computed with the Compton formula and σ is related to the position uncertainty (and not necessarily the position uncertainty).

The algorithm features some parameters to best adapt it to the experimental situation. These can largely affect the performance of the tracking and a certain emphasis will be placed in this topic in the course of the next Chapter. Table 1 contains a brief description of each of them together with their standard values (def.).

After the assignment of a merit factor, clusters are sorted and validated by requiring a merit factor above *minprobtrack* or *minprobsing*, if they consist of single interaction points.

PARAMETER	DEF. VALUE	FUNCTION
sigma_thet	0.25	Position resolution factor
minprobsing	0.15	Minimum probability to accept a cluster as a single interaction point
minprobtrack	0.05	Minimum figure of merit value to accept a cluster

Table 1: Description of OFT parameters. Def. values represent the standard parameters and will be used in the following chapter for reference.

At last, *sigma_thet* is a parameter that can be thought as a weighting factor on the test of equation 2: lower values will force more importance on the geometric position of the interaction and higher values will place more relevance on the remaining factors.

Figure 7, shows how the same data relative to different tracking parameters is affected by different combinations. In a spectroscopy experiment, the values are typically chosen to maximize the peak-to-total ratio, thus requiring the best separation between the peak and the background.

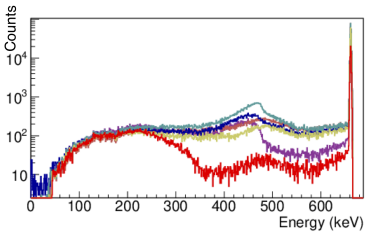

Figure 7: Different values of the parameters return widely different results of the tracked spectrum, changing the peak to total ratio as well as the counts in the photopeak.

Part II

TESTS OF FEASIBILITY

This section contains a detailed simulation of the response of the array to simulated emissions of single- and double-gamma events. The ability of the tracking algorithm to reconstruct the scattered photon is put to the test. A first approach to a new dedicated algorithm for this experimental challenge is discussed.

2 SIMULATION OF SINGLE AND DOUBLE-GAMMA DECAYS

The first step to undertake is the simulation of the response of the array at the isotropic emission of a single 661.7 keV gamma ray, relative to the $\frac{11}{2}^- \rightarrow \frac{3}{2}^+$ decay of ^{137}Ba. This test will quantify how many single gammas are wrongly tracked by the OFT algorithm as a function of the tracking parameters (Table1).

This simulation [13] of the response of the array is obtained in various steps:

- Events are generated randomly. Each event consists in a statement of various parameters such as the particle type, multiplicity, energy, direction of emission, position and velocity of the emitting source. In the current case an event expresses either the emission of a single photon or the simultaneous emission of two photons with fixed energy sum. The source is positioned at the nominal position, that is in the symmetry center, where the reaction target is usually located.
- Events are input in the AGATA Simulation code [12] which makes use of Geant4 together with the given geometry of the array to simulate stochastically the interaction of radiation with matter. The deposited energy as well as interaction position are returned if the particle has hit the detector at last.
- If multiple hits occur within 5 mm of each other, they are packed in a single interaction point by weighting the interaction position on the energy and adding the energies together.
- The energies of interaction are smeared by Gaussian distributions with an energy dependent relation [15] based on experimental data.
- At last, the OFT algorithm, modified to force the maximum clustering angle at 2π, clusters interaction points and generates a merit factor for each cluster. For each event, the algorithm returns a list of tracked gamma with their reconstructed energies and the position identified as the first hit. To cross-check the response of the tracking algorithm, the total energy deposited in each crystal of the array is included in the output.
- The tracked file is read by a scripted function and later analyzed to produce histograms and graphs in the ROOT data analysis framework.

The position smearing present in the OFT simulation code showed issues in its output, moving a consistent number of points outside the detector, up to 200 mm away from its surface.

This problem could be observed about once every 10^4 events.

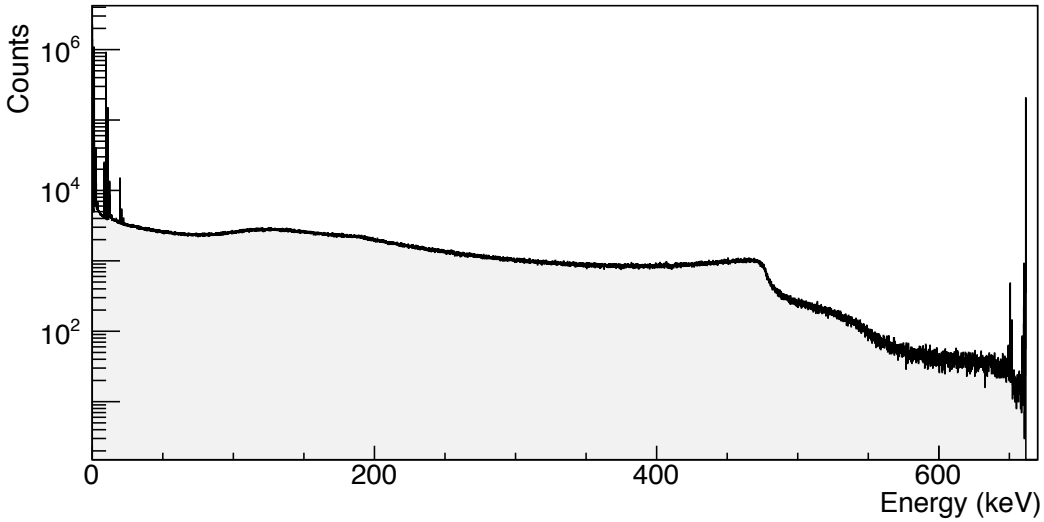

Figure 8: Histogram of the energy (with infinite resolution) deposited in every hit for the 661.7 keV photon, when simulating the AGATA array in its current configuration. At low energy peaks corresponding to the X-rays of Ge are present. A peak slightly lower than the main full energy peak is also visible. This consists in multiple peaks which correspond to an energy equal to $661.7 - E_x$ keV, where E_x represents one of the X-rays of Germanium. In fact, with a lower cross section, the photon can be absorbed by a more binded electron.

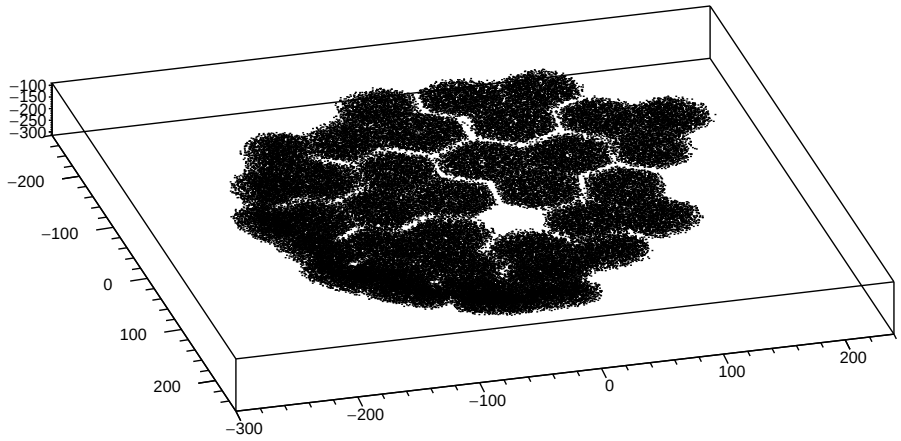

Figure 9: Interaction points in 3D space, the graph shows the geometry of the array and a uniform distribution of the hits.

As a consequence the smearing was disabled, relying on the packing of the interaction points and the energy smearing for the realism of the simulation. This certainly returns optimistic results compared to a real experiment. The energy dependence of the position resolution in the AGATA detectors has been studied by Söderstorm et al. [15] and consist in a Gaussian distribution with an energy

dependent FWHM. The influence of this position smearing on the performance of the tracking can be studied in further works.

Figure 8 shows the deposited energy by a 661.7 keV gamma before the energy smearing and shows the spectrum of a Germanium detector with infinite energy resolution. The graph is useful to understand some absorption processes simulated. The low energy peak corresponds to the X-rays of Ge. The peak at the incident gamma ray energy corresponds to a gamma ray which is absorbed by photoelectric effect in the first interaction. As one can observe in Figure 2, 600 keV is the region of transition between dominant photoelectric absorption and Compton scattering, as a consequence the full absorption peak is present.

Figure 9, on the other hand simply shows the interaction points in three dimensional space, highlighting the geometry of the array and its triple-cluster structure.

2.1 GENERATING DOUBLE-GAMMA EVENTS

Double-gamma decay events have been generated with the correct angular and energy distributions. These observables depend on the transition multipolarity combination and each has its branching ratio. In the case of ^{137}Ba the M2-E2 and M1-E3 transitions are those which contribute most, as argued in reference [3].

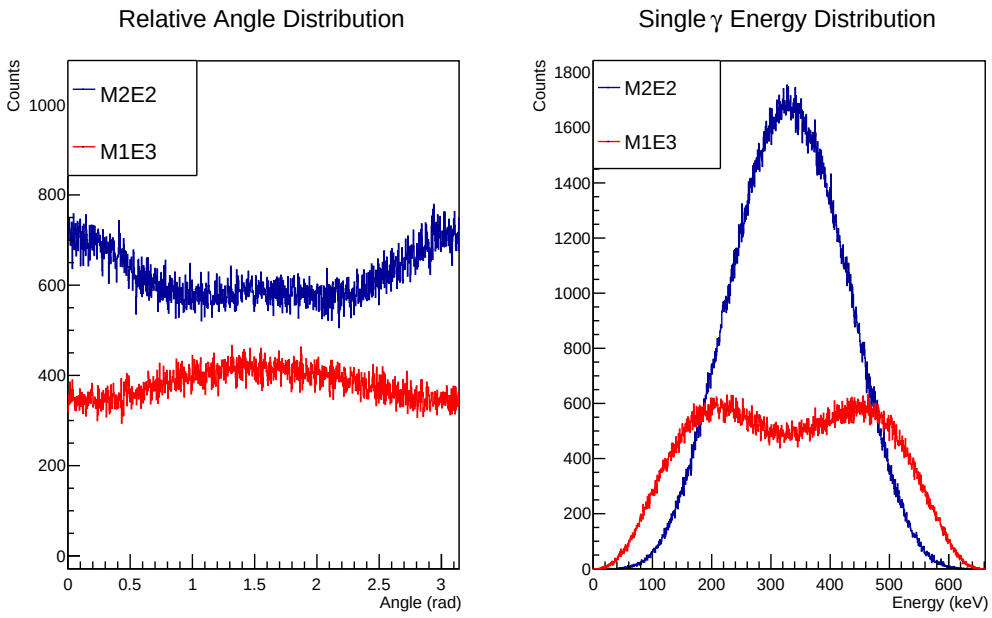

Figure 10: Angular and energy distributions for the two main transition multipolarities.

To generate the events, the built-in random generator of ROOT was used. This has a period of $2^{19937} - 1$, well above the number of simulated events, and proved to be fast enough for its scopes. In the code, an event is generated as follows:

- A random versor $\hat{x}_1$ in 3D space is generated with an isotropic distribution

- By sampling from a uniform distribution, based on the branching ratio, the type of event is chosen. For ^{137}Cs the main events are three (single gamma (M4), double-gamma (M2-E2) or (M1-E3)):
  - *Single Gamma*: The direction of the gamma is that of $\hat{x}_1$ and the energy is that of the transition.
  - *Double-gamma*: The multipolarities of the gamma transitions are asserted (quadrupol-quadrupole or dipole-octupole), the energy of the first gamma E_1 is sampled from the energy distribution of the given transition (Figure 10 (right)) while the other energy is fixed by $E_{tr} - E_1$. An angle α is sampled from the angular distribution (Figure 10 (right)) and another random 3D versor $\hat{x}_2$ is generated. The first gamma is assigned E_1 and $\hat{x}_1$. The second gamma is assigned the fixed energy and a position computed by $R(\alpha, \hat{v})\hat{x}_1$, where R is a matrix which rotates $\hat{x}_1$ by an angle α around $\hat{v} = \hat{x}_1 \times \hat{x}_2$.
- Each event is written into a file respecting the format required by the external event generator from the AGATA simulation code.
- The code has an option to plot a distribution of the generated events to check the soundness of the algorithm.

By generating exclusively double-gamma events (with M2-E2 or M1-E3 multipolarities) one can obtain the distributions shown in Figure 10. The distributions have different areas, due to the fact that an M2-E2 transition is more likely to occur.

2.1.1 *Quantifying the performance of the tracking*

By not taking into account the timing of events (no random coincidences) and not considering the radiation background, as well as many other experimental aspects, this test is meant as the ideal case scenario for the measurement, and yet it returns many informations on the current limitations of the array. While it is certainly possible to include background as well as other experimental aspects in the simulation, the choice of attaining to the simplest case was made to benchmark the performance of the tracking on its own.

Different values of the parameters described in section (1.5.2) affect the outcome, as one can bias the algorithm towards uniting events and also induce a higher discard rate due to more strict requirements.

However, requiring more severe conditions hinders the measurement of the real double-

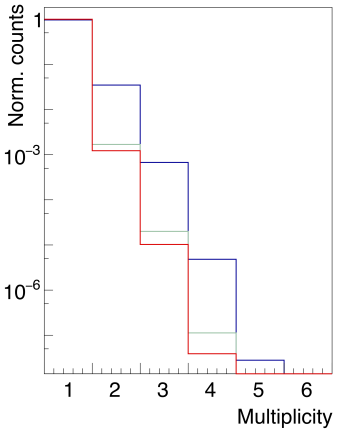

Figure 11: Tracked multiplicity of the simulated single gamma. In blue the default parameters, in red the optimal combination and in green the second best (Section 2.2).

gammas by inaccurately merging together interaction points belonging to separate photons.

Figure 11 represents the multiplicity returned by the tracking algorithm with the condition of a total energy within 2 keV from the transition energy, when only the emission of a single gamma is simulated. Together with the default parameters (Table 1), the graph shows data relative to the optimal parameters found in Section 2.2. Multiplicity two events as well as even higher multiplicity photons are found, even if only a real single gamma is simulated.

This aspect in itself represents the major obstacle in the measurement of such a low branching ratio event such as the competitive double-gamma decay.

From a graphical perspective, it is hard to represent the effect of three parameters, however limiting to *minprobsing* and *minprobtrack*, it is possible to obtain the two dimensional plots in Figure 12. These are relative to the tracking of the same set of 1 million simulated events with a total of 900 different combinations of the two parameters in intervals centered around the claimed typical value (Table 1) and with the default *sigma_thet*.

For instance, by increasing the value of *minprobtrack*, one expects a lower number of falsely tracked single gammas as the code is requiring a higher confidence to accept an event, and this is the case in Figure 12 (top left, top right). If no combination is able to reach the desired merit factor, the tracked event is discarded and only the total energy deposited in the corresponding crystals is sent to the output. In this case AGATA is treated as a traditional non-segmented HPGe array. Since *Sigma_thet* is related to the error in position of the array and serves as a weighting parameter to bias the algorithm towards placing more importance in the Compton constrain of the merit factor, low values are expected in applications where tracking precision is crucial.

The number of multiplicity one events is also decreasing for high values of both parameters (Figure 12 (bottom left)) as the high thresholds are prompting the algorithm to reject more events. At last, the peak to total (bottom right) is maximized for high values of *minprobsing* and lower values of *minprobtrack*.

The region where the tracking is recognizing most single gammas as fold 1 corresponds to high values of both parameters. In fact while a high *minprobtrack* requires a low uncertainty for the event to be accepted, a high value of *minprobsing* means single interaction points are unlikely and thus the algorithm is trying to aggregate as much as possible the hits.

On its own, the rejection of the incorrectly tracked single gammas does not hold much significance, as the tracking performance of double gammas has not yet been taken into account.

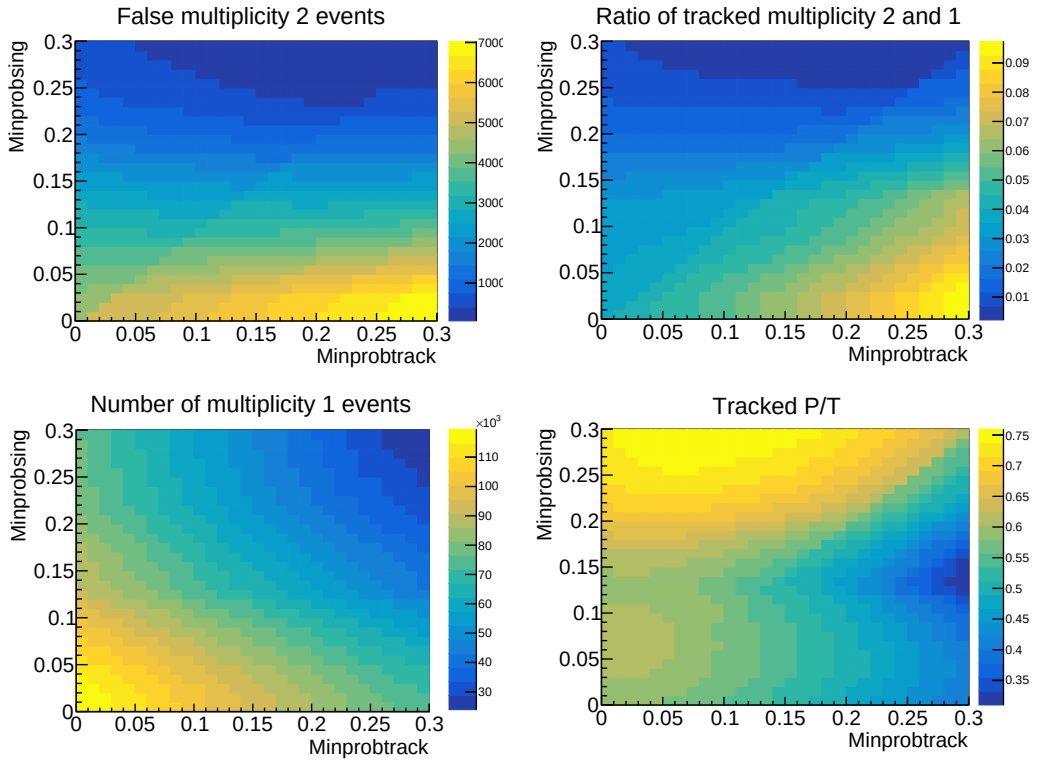

Figure 12: Various outputs of the tracking as a function of *minprobsing* and *minprobtrack*. As the parameters are three, this graph only serves as an example as the value of *sigma_thet* is fixed throughout.

2.2 OPTIMIZING THE PARAMETERS

In order to optimize the tracking parameters, the same number of double and single gamma events have been tracked with a different combination of parameters within the intervals stated in Table (2). A total of 3×10^6 events for both single and double gammas were used as input for the tracking algorithm. The chosen number of events was decided by taking into account that some of the combinations of parameters were rejecting a considerable amount of events.

Despite the known issue on the position smearing, the choice was made to keep it enable during the optimization, thus avoiding unrealistic parameters especially for *sigma_thet* which is related to the position uncertainty.

A reconstructed event was selected as either a wrongly tracked single gamma or a correctly tracked double-gamma if the energy sum was within 2 keV from the transition energy and the distance between the first interactions of the two reconstructed photons was above 125 mm, as a large fraction of incorrectly tracked single gammas populates this region (Section 2.5).

Table 2 records the optimal values as found by the described procedure. As the value of the ratio is not affected by rapid variations, a more complex maximum-searching algorithm was not considered any more beneficial compared to a simple grid search.

PARAMETER	MINIMUM	MAXIMUM	STEP	OPTIMAL
sigma_thet	0.3	5.8	0.5	0.8
minprobsing	0.05	0.4	0.05	0.4
minprobtrack	0.05	0.3	0.05	0.15

Table 2: OFT parameters intervals. The value of *minprobsing* corresponds to the interval edge, however allowing for an even higher value might lead to unrealistic results.

2.3 CONSIDERATIONS ON THE REJECTION RATIOS

Since the double-gamma decay is characterized by continuous distributions, it's search is not limited to finding a peak. One expects a background distribution (noise generated by Compton events or natural background) summed with the expected double-gamma distribution. The data analysis consists in estimating the background and subtracting it to the data in order to observe the distribution. Intuitively, to do so, the integral of the signal and noise distribution must be of the same order of magnitude.

Since the number of single and double gammas produced in the event generator will not be the same in the following analysis section, the *rejection* ratio R between measured and generated events must be used in future considerations. Only events where the full energy has been deposited in the array are considered, by requesting a total energy within 2 keV of the transition. It is useful to define $N_{o,i}$, where $i = \gamma, \gamma\gamma$, as the number of observed multiplicity two gammas when one ($i = \gamma$) or two ($i = \gamma\gamma$) photons are simulated.

$N_{o,i}$ is proportional to the detector calorimetric efficiency ϵ corresponding to the ratio between gammas that have fully deposited their energy in the array and the number of photons emitted N. In a measurement (or a simulation), the intensity of the source (number of simulated events) is known, as well as the number of detected photons $N_{o,\gamma}$, which can be extracted from the spectrum of the energy of the sum of the cores.

The value of the efficiency ϵ depends on the event type (single or double gamma). At last, the rejection ratio R depends on the performance of the tracking: relative to its probability to reconstruct incorrectly one gamma in two gammas (R_γ) or to correctly track two gammas ($R_{\gamma\gamma}$). Thus the following relation holds for single gammas tracked with multiplicity two:

$$N_{o,\gamma} = R_\gamma \, N \, \epsilon_\gamma$$

The number of measured double-gammas with branching ratio $BR_{\gamma\gamma} = \Gamma_{\gamma\gamma} / \sum_i \Gamma_i$ is thus given by:

$$N_{o,\gamma\gamma} = R_{\gamma\gamma} \, N \, BR_{\gamma\gamma} \, \epsilon_{\gamma\gamma}$$

Requiring a ratio between single gammas incorrectly tracked as multiplicity two and double gammas tracked correctly of approximatively one, yields the condition:

$$BR_{\gamma\gamma} = \frac{R_\gamma \epsilon_\gamma}{R_{\gamma\gamma}\epsilon_{\gamma\gamma}} \left(\frac{N_{o,\gamma}}{N_{o,\gamma\gamma}} \right) \approx \frac{R_\gamma \epsilon_\gamma}{R_{\gamma\gamma}\epsilon_{\gamma\gamma}} \tag{3}$$

This condition states that the ratio defined in equation 3 represents a good benchmark for the sensitivity to the competitive double gamma decay process.

2.4 HOW MUCH ARE THE RESULTS AFFECTED

The scope of the tracking is to reconstruct the path of the gamma ray inside the HPGe shell in order to extract its energy from its different interaction points in the crystals. The tracking allows to reconstruct part of the Compton scattered events, thus reaching P/T capabilities similar to a Compton-suppressed array while considerably increasing the detection efficiency due to the absence of Compton shields. However, by changing the tracking parameters which include some acceptance thresholds (Table 1), one can also inadvertently introduce significant biases on the measured quantities. One way to test this aspect is to consider the energy distribution of one of the two tracked double-gammas with the optimal parameters found and with the default parameters. Figure 13 shows the distribution generated by the event and what is observed by setting different tracking parameters.

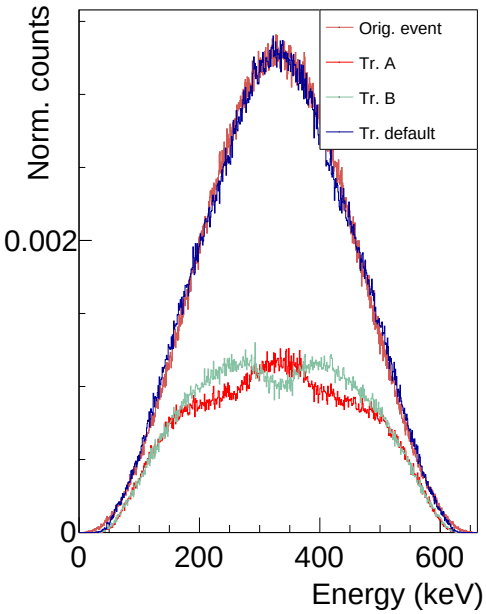

Figure 13: Energy distribution of double gammas with M2-E3 and M1-E3 multipolarities. In blue the measured distribution with the default parameters together with the distribution with optimal parameters (red), and another combination showing similar performance (green) (Table 2).

While the original events and the default parameter spectra have been normalized to be comparable, the remaining spectra with the optimal parameters (Table 2), have been normalized with the same constant as the default spectrum (blue). This allows the comparison of the energetic intervals where the tracking is applying a bias by either rejecting double-gamma events or merging them together.

In fact, the central energy region is more affected by this bias, which decreases moving away from the symmetry axis. This bias, however, can be predicted by a simulation and be used to reconstruct the original distribution. Many other graphs are affected by the tracking conditions but, notably, the angular distribution does

not show significant differences and is mainly affected by the geometry of the array.

The spectrum was generated by picking randomly the first or second of the tracked gammas if their sum was within 2 keV from the transition energy.

2.5 ANALYSIS OF THE SIMULATION

In the following section, a quantitative analysis of the simulated data will be discussed. The data is generated by simulating 1×10^8 double-gamma events and 1.339×10^9 single-gamma events tracked with the parameters found in the previous chapter.

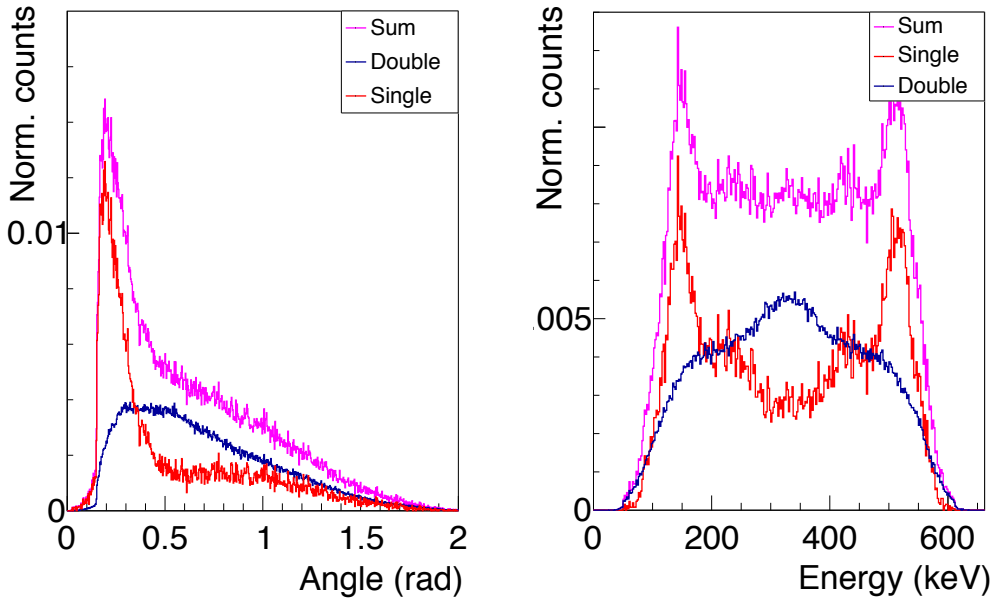

(a) (b)

Figure 14: Normalized distributions for simulated single and double-gamma events tracked with multiplicity two and energy condition (equation 4). (a) Angular distribution, at small aperture angles: many single gammas are incorrectly tracked while many double-gammas are merged into a single event. At very low aperture, the minimum clustering angle defined in the tracking algorithm automatically unites the interaction points. (b) Energy distribution, single gamma events present two peaks due to Compton back-scattering.

Most graphs have been normalized to make comparison possible. It is to be noted that the found parameters are lowering considerably the number of reconstructed gammas to bias the array towards a more precise event reconstruction.

Figure 14 shows the energy and angular distributions for both single and double gamma events. As introduced in Section 2.3, to exclude photons which have

deposited some energy in the crystal and later escaped detection via Compton interaction, a condition on the total energy of multiplicity two events was set:

$$|E_1 + E_2 - 661.7 \text{ keV}| < 2 \text{ keV} \quad (4)$$

The energy distribution was generated by selecting randomly between first and second tracked photon, as the OFT algorithm, due to its merit factor ordering and selection procedure, does not order randomly the events, generating an asymmetric histogram. While the energy distribution is mainly affected by the tracking, as seen in the previous section (2.4, Figure 13), the angle distribution depends also on the geometry of the array as little solid angle coverage is available for events with large aperture due to the available detectors in the AGATA array. At the same time, small angles can not be reconstructed due to limitations on the position precision of the array and notably due to the tendency of the tracking to merge nearby clusters. Small-angle events (< 0.4 radians), however, mainly consist in single 661.7 keV gammas reconstructed as fold two events.

It is important to identify classes of events that are commonly tracked inaccurately by OFT. This translates into identifying and excluding regions of various graphs where many single gammas are inaccurately tracked as double as well as locating regions where double-gammas mostly concentrate.

The angular distribution (Figure 14 (a)) clearly shows that events with aperture below 0.4 radiants can not be measured due to the high number of single gammas tracked with fold 2. However, the measured aperture does not take into account one dimension, the depth of the interaction. As a consequence, the best choice is to introduce the distance between tracked points (Figure 15). As many single gammas concentrate for distances below 125 mm, the parameter optimization was performed for distances above this threshold.

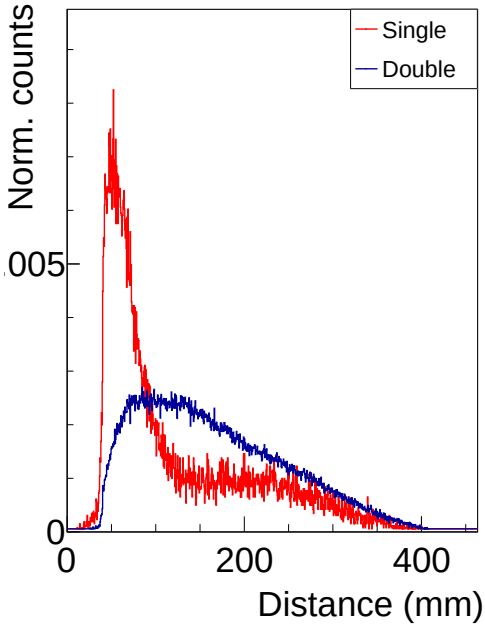

Figure 15: Distance between multiplicity two tracked events.

As the photon absorption is characterized by an exponential decay (Section 1.3), a similar trend would be desirable in the plot; however a pronounced tail is present at high distances. The exponential absorption is evident only in the first 100 mm of Germanium.

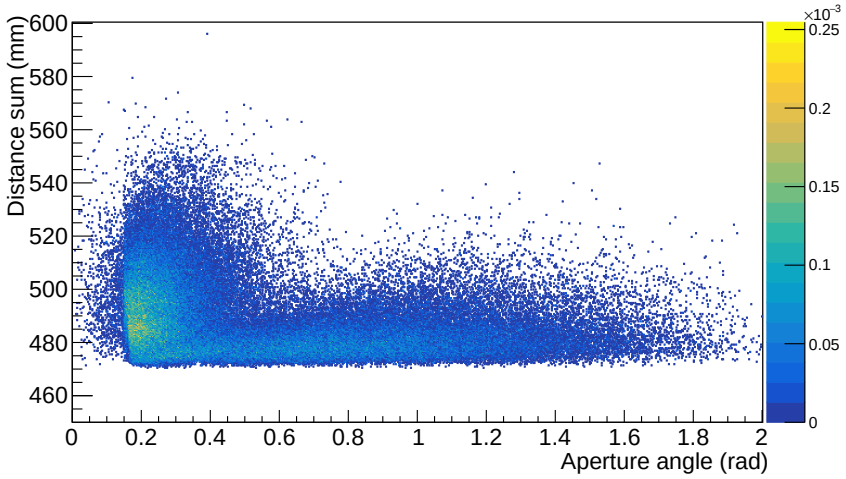

(a) Single 661.7 keV photons

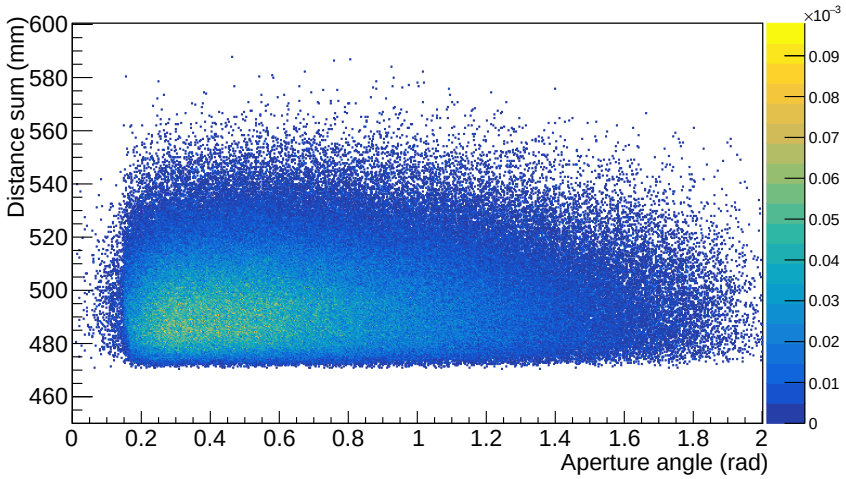

(b) Double-gammas

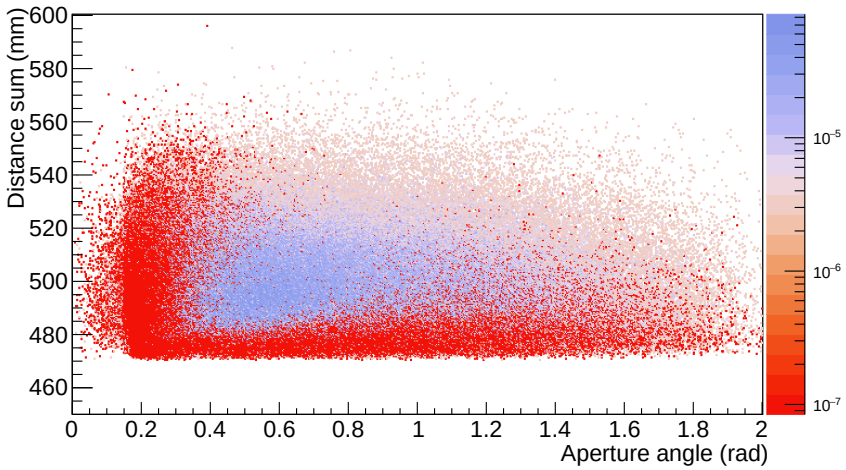

(c) Difference histogram

Figure 16: Normalized matrices of the aperture angle and the distance between the first interaction and the source for single (a) and double-gamma (b) events. (c) is the difference between the normalized matrices and highlights in the blue region a double-gamma prevalence.

This is explained by the somewhat spherical geometry of the array, as photons can easily scatter from one side to the other of AGATA, thus being registered with large aperture while passing only through air.

Plotting the sum of the interaction depths and the aperture angle proves this point since, for single events, photons that interact further in depth in the germanium are less likely to scatter back to the other side, having lost a considerable amount of energy via Compton effect (Figure 16).

To identify and quantify events, two dimensional plots can be created for single and double-gamma events (Figures 16, 18 and 19). After the normalization of the histograms, a subtraction between graphs relative to the double and single-gamma simulations will be performed (panels (c)). The two-dimensional difference plot is shown in logarithmic scale on the z axis to highlight the regions of interest. Negative regions are shown in solid red and correspond to areas where a high amount of incorrectly tracked single gammas are present.

Double-gamma events are less energetic compared to the single gamma counterparts. As a consequence, the absorption cross section is higher and, on average, they interact more on the surface of the detector, thus completely excluding this region in Figure 16 is not a viable choice. Nonetheless, a clear region of interest, which is not considerably affected by the tracking parameters, emerges. In fact, using the default tracking values, yields a figure with higher statistics and a similar difference plot.

Another consideration can be taken regarding events that are likely Compton scattered single gamma simulated photons. By plotting the scattering angle between gamma rays and the energy of the second gamma, one can obtain a graph similar to Figure 17. The latter is relative to a simulation of single gammas transitions tracked using the default OFT parameter values. The definition of this graph leaves an uncertainty as the event time order is unknown, the choice is made depending on which combination returns the best similarity to the Compton formula in absolute value. The red line in overlay shows the Compton formula of equation 1.

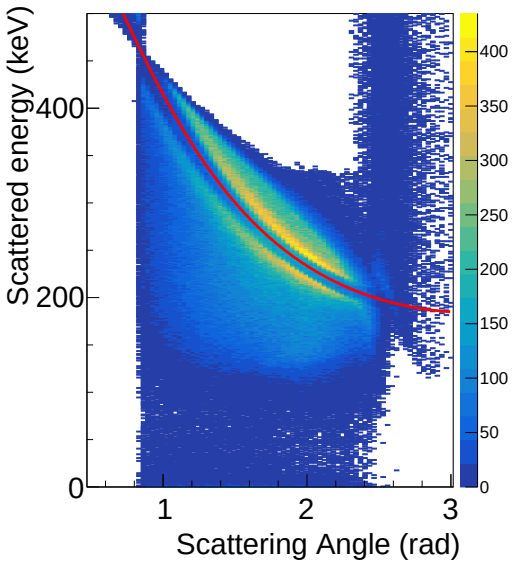

Figure 17: Scattering angle and scattered energy of single gamma events tracked as fold 2 with default OFT parameters.

Clearly, the tracking algorithm is able to recognize Compton scattered photons in proximity of the line described by equation 1, where a valley is present. However, the highest concentration of badly evaluated events still resides nearby the formula if the default OFT parameters are used.

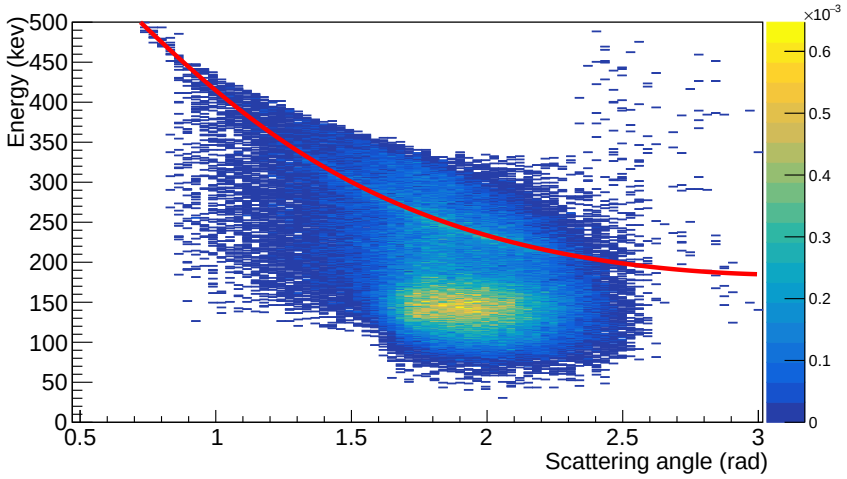

(a) Single 661.7 keV photons

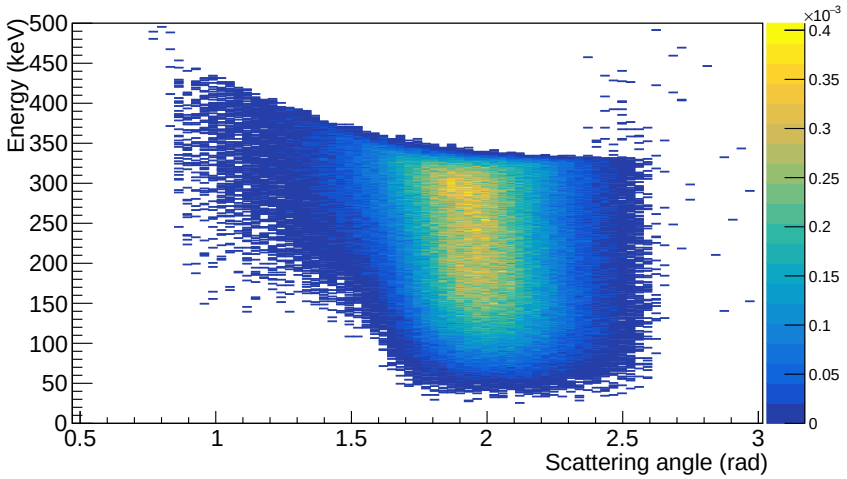

(b) double-gammas

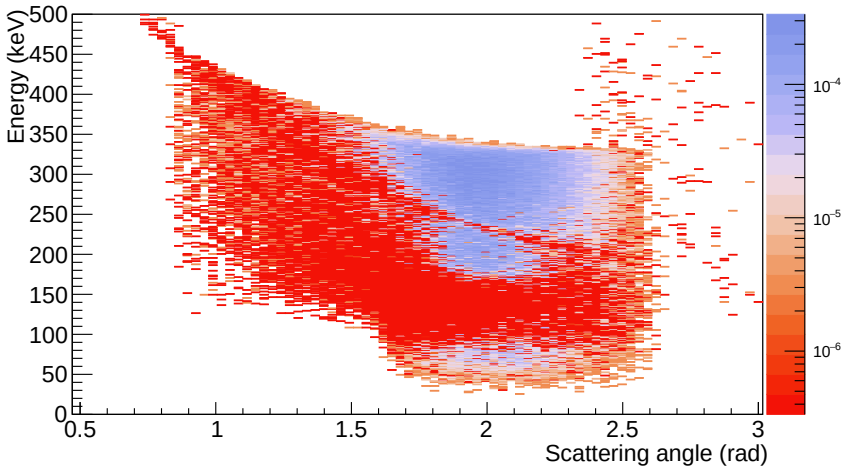

(c) Difference matrix

Figure 18: Normalized matrices of the scattering angle and the energy of the scattered photon for simulated single (a) and double (b) events. The Compton-scattered photon is chosen as the one which most closely follows equation 1. (c) is the difference between the normalized matrices and highlights in blue regions of double-gamma prevalence.

The same graph can be generated for single and double-gamma events with the optimal parameters set (Figure 18).

In this case the distribution of the incorrectly tracked photons is more regular and uniform and no patterns are found near the Compton formula. Unfortunately the region of high concentration of mistakes tends to coincide with a very similar region of prevalence of double-gammas correctly tracked.

The difference of the normalized plots shows a double-gamma preponderance area between the scattering angles of 1.7 and 2.6 radians.

Plotting a 2 dimensional histogram with the energy difference between the gamma and the aperture angle with respect to the source also reveals some information. Calling $x = E_1 - E_2$ and knowing that $E_1 + E_2 = E_t$ ($E_t = 661.7$ keV) (energy condition 4), one can reformulate the Compton formula as:

$$\theta = \arccos\left(1 - \frac{4m_e c^2 x}{E_t^2 - x^2}\right)$$

Where θ is the usual scattering angle. Relating the latter with the aperture angle is not trivial as they are not mapped by a one to one relation, meaning that for a given scattering angle many aperture angles correspond and vice versa. This will create a distribution, and it is to be expected that such distribution will be centered around the symmetry of the system. For symmetry reasons, a rough estimate of this condition is the following, obtained by requesting a scattering angle θ on an isosceles triangles with aperture α:

$$\theta \approx \frac{\pi + \alpha}{2}$$

The top red line in the Figure 19 (a) corresponds to this relation and proves that the ridges present are mainly due to back scatter events from one side of the array to the other. At lower aperture angles, this configuration cannot be observed as the photon which interacts in the detector, scattering at high angles and low apertures only passes through Germanium.

For the double-gamma graph, in principle one would observe on the x-axis the relative angle distribution of Figure 14 and on the y-axis a distribution similar to that of the energy of one of the emitted gammas. Formally, if $f_E(E_1)$ is the distribution of the energy of the photon and $f_x(x)$ is the distribution of the energy difference, the change of variable $x = g(E_1) = E_1 - E_2 = 2E_1 - E_t$ generates the following energy difference distribution, which is observed in the y-axis projection:

$$f_x(x) = \left|\frac{d}{dx} g^{-1}(x)\right| f_x\left(g^{-1}(x)\right) = \frac{1}{2} f_E\left(\frac{x + E_t}{2}\right)$$

The energy difference of the normalized histograms shows regions to avoid nearby the ridges and for small aperture angles while locating a prevalence of well tracked double-gammas in between these regions, negative areas are marked in red.

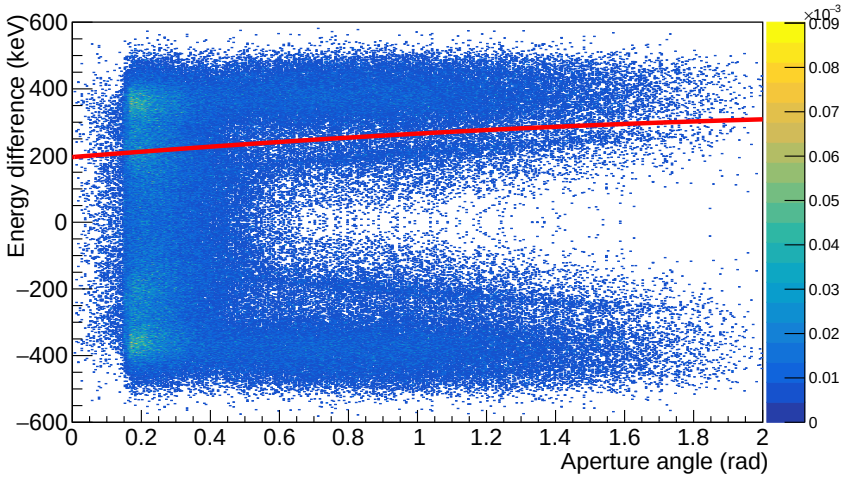

(a) Single 661.7 keV photons

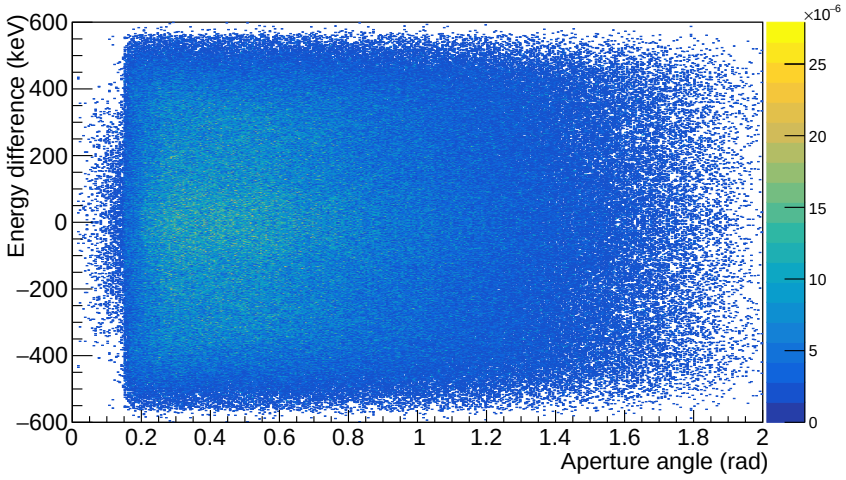

(b) double-gammas

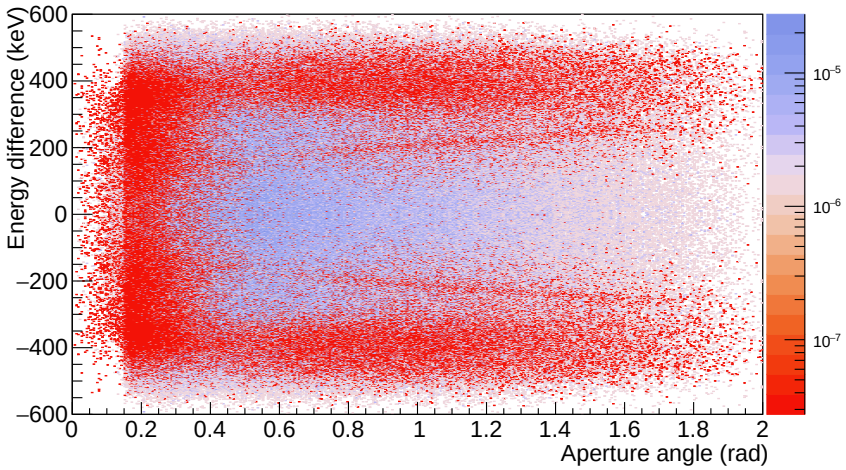

(c) Difference histogram

Figure 19: Normalized matrices of the aperture angle and the energy between the tracked gammas for single (a) and double (b) events. (c) is the difference between the matrices and highlights in the blue region the double-gamma prevalence.

2.5.1 *Event selection*

It is possible to operate a selection on the events on a two dimensional graph. These techniques are often called graphical cuts and will be operate in regions where mostly correctly tracked double-gammas are present. By doing so, a better rejection ratio is expected, while hopefully losing few information on the double-gamma decay.

Regions marked in red in Figures 16 (c), 19 and 18 will be avoided, so that regions of double-gamma data prevalence will be measured.

Table 3 reports a summary of the final results of the procedure described in this Section.

EVENT TYPE	ϵ	$R_i\,\epsilon$	$R'_i\,\epsilon$	R'_i
γ	8.97×10^{-2}	7.04×10^{-5}	3.81×10^{-6}	4.24×10^{-5}
$\gamma\gamma$	1.78×10^{-2}	3.27×10^{-3}	1.15×10^{-3}	6.47×10^{-2}
Ratio $\gamma/\gamma\gamma$	5.04	2.15×10^{-2}	3.31×10^{-3}	6.55×10^{-4}

Table 3: Final simulation ratios after event selection with 1.339×10^9 single gammas simulated and 1×10^8 double-gammas with the optimal parameters. The last line corresponds to the conditions found in equation 3 and need to be confronted with the branching ratio.

While the efficiency ϵ is the calorimetric efficiency for the 661.7 keV photons which fully deposit their energy in the array (within 2 keV, as defined in Section 2.3) and R represents the rejection ratio defined in the same section, R' is the ratio after the event selection procedure. Thus, the second column presents the percentage of observed double-gammas for a single and real double-gamma event after the tracking. This depends on the rejection ratio of the algorithm as well as ϵ, since an inferior number of double-gammas fully deposits its energy in the array in the current setup while $\epsilon R'$ is the percentage of double-gammas detected after the graphical cuts.

Notably, the last column states the ratio of detected single gammas and double gammas if the two event types were to have the same calorimetric efficiency. After the event selection, the tracking algorithm is discarding 35.3% of the double gammas while only 0.00424% of single events is reconstructed as two photons.

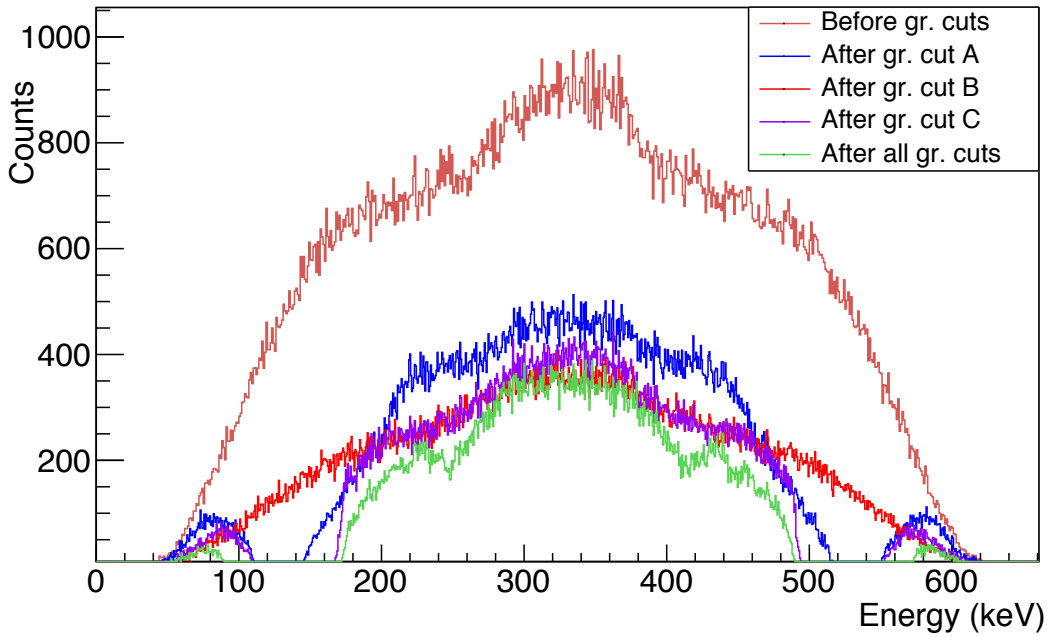

Figure 20: Spectrum of one of the two double gammas tracked before and after graphical cut A (Figure 18), after cut B (Figure 16) and after cut C (Figure 19). Many events are lost due to the poor separation between single and double-gammas, in green the final distribution.

While graphical cuts are able to improve by one order of magnitude the ratio, they are also destructive for the measurement of the data itself. In fact, plotting the single photon energy distribution of a double gamma event before and after the graphical cut alters the expected distribution. Figure 20 shows the effects of the cuts labeled as follows:

- A: Figure 18 (energy of the scattered gamma and scattering angle)
- B: Figure 16 (distance sum and aperture between the gammas)
- C: Figure 19 (energy difference and aperture angle)

Cut A and C, operate directly on the energy of the gamma, thus having a large impact on the distribution compared to cut B. On the other side, cut A is able to reject 38% more single gammas compared to B and so contributes in larger part to the final rejection ratio.

2.6 FUTURE PERSPECTIVES

In which direction should further developments focus on if the final goal is the measurement of the double-gamma decay, i.e. a very low branching ratio event? Many options are possible, most of them are not simple to achieve:

- *An improvement of the PSA resolution*: the tracking would benefit greatly from an improvement of the position resolution, since hits that occur near to each

other are affected by high scattering angle uncertainty. This can be tested in further simulations up to an arbitrary precision.

- *A leap forward in the tracking algorithm*: testing other options might reveal beneficial, including a more complex statistical analysis, or the improvement of the position error estimate. Some new developments focus on this aspect, by making use of a more complete statistical analysis, namely Bayesian methods, to refine the algorithm precision ([23, 24])
- *A full solid angle coverage of the detector*: the completion of the full angular coverage of the array is planned and, from the point of view of this measurement, might be essential.

This last point will be briefly discussed on the next section 2.6.1.

2.6.1 *AGATA* 4π

This setup would allow for measurement of relative angles between 0 to π radians and a higher double-gamma detection efficiency. In fact, in the previous simulation, double-gammas were affected by a lower efficiency as both of the photons needed to end up in the covered solid angle. In the case of full solid angle coverage, the double-gamma full energy deposition is increasing substantially more than the single gamma efficiency.

Thanks to the higher detection efficiency, a total of 7.68×10^7 single gammas were simulated ($\epsilon_\gamma = 0.522$) as well as 3.00×10^7 double-gammas ($\epsilon_{\gamma\gamma} = 0.325$). A quick check was performed to identify the best parameter values, by using the same parameter intervals (2) but limiting *sigma_thet* below or equal to 1.8. The identified values were: *sigma_thet*= 0.8, *minprobtrack*= 0.15 and *minprobsing*= 0.4.

In Figure 21 the equivalent graphs of Figures 16, 18 and 19. A more clear event separation is evident, thanks to the higher angular acceptance. Notably the same trends are evident; Figure (a) shows a similar region of incorrectly tracked single gammas and the same can be said for the remaining plots.

This data is intended as a mere test of the concepts applied in the previous section and a more precise analysis should be performed with the full array.

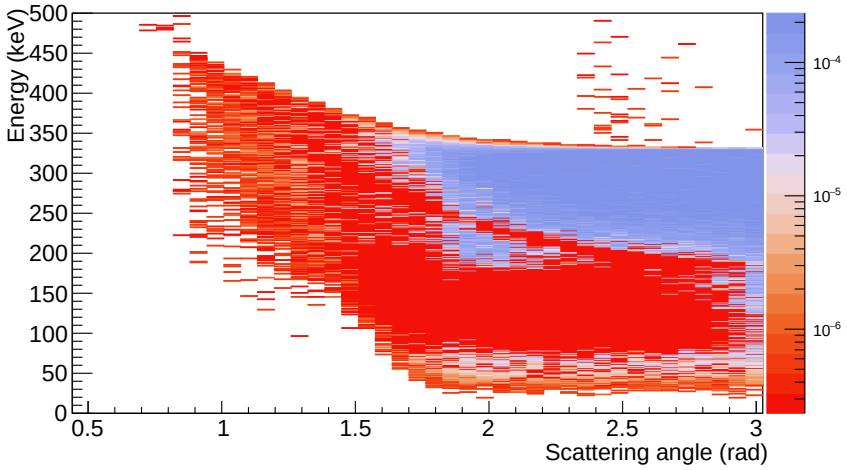

(a) Single 661.7 keV photons

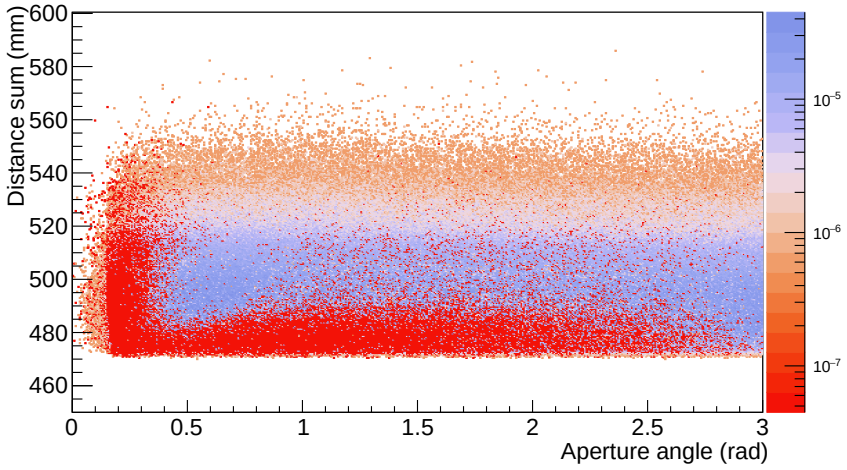

(b) double-gammas

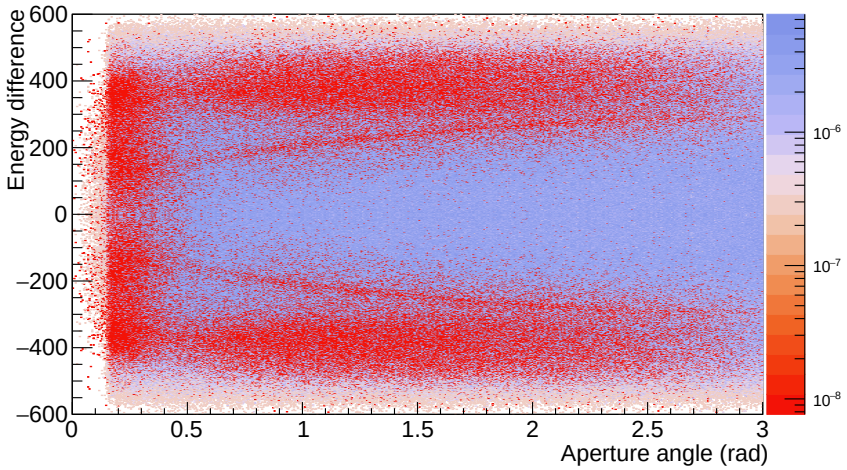

(c) Difference histogram

Figure 21: Analogous graphs of Figures 16, 18 and 19, consisting in the difference of normalized graphs of single and double-gammas for the full array AGATA 4π. Regions marked in solid red corresponds to a prevalence of incorrectly tracked single gammas.

2.7 A DIFFERENT MERIT FACTOR FOR THE DOUBLE-GAMMA ANALYSIS

Due to the results of the previous section a new approach was investigated for the analysis process. From a concrete standpoint, the project can be thought as a first implementation of a new algorithm and from a statistical point of view, a new direction was searched. While its intent is not to replace the current algorithm, its purpose is to test if a more precise understanding of the event selection of double-gammas events can be reached. As a consequence, the code is not versatile as its only focus is to compute the merit factor for single or double events and, by disabling the clustering procedure and testing all permutations, its analysis is more resource demanding. Due to time constrains, the algorithm [25] was not thoroughly tested and characterized, many improvements can and should me made on the event thresholds. Numerical integration should be introduced in the future for double events which have passed the selection test. While the algorithm is now running considering the array as a spherical shell, the geometry can be included in the computation of the distance in germanium of the first hit, by including the position of the center of the faces of the crystals (similarly to what is done in the new implementation of OFT). While this function has not been used, it could also be extended to compute the distance in germanium between different hits, by including the position of the corners of the crystals. This possibility has not been included yet, as the code must be thought as a work in progress.

Considering a photon interacting N times inside the array, with $N-1$ Compton scattering events and a final photoelectric absorption, the probability related to the event $\mathcal{P}_s$ can be approximated by the formula:

$$\mathcal{P}_s = \prod_{i=1}^{N-1} \left(\frac{d\sigma_c}{d\Omega_i} \exp(-n\,\sigma_{c,i}\,r_{ge,i}) \right) n\,\sigma_{ph,N}\,\exp(-n\,\sigma_{ph,N}\,r_{ge,N}) \tag{5}$$

Where σ_c is the Compton cross section and r_{ge} is the distance in germanium that the gamma ray passes, n the numerical density and σ_{ph} the photoelectric absorption cross section. These quantities depend on the stochastic variables $\hat{E}$ and $\hat{x}$ which are constrained by the Compton formula. If the position and energy errors are Gaussian, the distributions are a function of the measured energy and positions (E_i and $\mathbf{x}_i$) the form:

$$\mathcal{P}_n = \exp\left(-\frac{|\mathbf{x_i} - \hat{\mathbf{x}}_\mathbf{i}|^2}{\sigma^2_{x_i}} \right) \exp\left(-\frac{(E_i - \hat{E_i})^2}{\sigma^2_{E_i}} \right) \tag{6}$$

$\mathcal{P}_n$ is independent on the path order and should be constant in every permutation, moreover it does not contain the integration variables $\hat{x}$ and $\hat{E}$. Numerical integration over the random variables should return a likelihood for each possible path. This feature is not yet implemented. To test the algorithm, the random variables, in first approximation, were replaced by the measured values in equation 5. A discrimination factor ($\mathcal{P}'_n$), similar to the one in OFT (equation 2), was added in place of equation 6. In this case σ (equation 2) corresponds to an error on the energy of the scattering photon computed by propagating the error of the cosine:

$$\cos(\theta_{i-1,i,i+1}) = \frac{(\mathbf{x}_i - \mathbf{x}_{i-1}) \cdot (\mathbf{x}_{i+1} - \mathbf{x}_i)}{|\mathbf{x}_i - \mathbf{x}_{i-1}|\,|\mathbf{x}_{i+1} - \mathbf{x}_i|}$$

And the final error on $E(\theta)$:

$$\delta E = \left|\frac{\partial E}{\partial \theta}\delta\cos(\theta)\right| \quad \text{where} \quad \delta\cos(\theta) = \sqrt{\sum_{\alpha=\{i-1,i,i+1\}} \nabla_{\hat{\mathbf{x}}_\alpha}\cos(\theta_{i-1,i,i+1})\cdot\delta\hat{\mathbf{x}}_\alpha}$$

Where the error on the i^{th} component of the position is found from the general error position δr as: $\delta\hat{\mathbf{x}}_{\alpha,i} = \delta r/\sqrt{3}$. At last, in the current implementation, $\mathcal{P}_s$ and $\mathcal{P}'_n$ are multiplied to obtain the final merit factor. This factor is rescaled on the number of interaction points. This means that the merit factor is still not optimal as in the ideal case the number of interaction points should count as discriminating factor in the event selection.

With the current limitations, by setting a condition on the ratio of merit factors between single and double-gamma events it is possible to obtain rejection ratios in the range of $[10^{-1}, 10^{-2}]$. While these results are still very preliminary and approximations within the code are still rough, they represent a first step in the development of a dedicated algorithm for the study of the competitive double gamma decay. A more complete approach from a statistical and operational standpoint is under development [23, 24].

2.7.1 *The code*

The tracking code was developed in C++ to take advantage of an abstract implementation through classes and a fast runtime, without any significant downsides.

One of the main challenges in developing the algorithm was to avoid to compute multiple times the same quantity. This is not a simple task for this algorithm as each vertex of interaction depends on the previous two. Permutations were thus computed in lexicographic order and the merit factor relative to the path was recorded at each step, in order to be able to recover the computed data.

2.7.2 *Needed developments*

Due to the discrete position resolution of the array, it is possible for a Compton scattered gamma ray to lose most of its energy in the process and to be later absorbed by photoelectric effect nearby, too close for the detector to be able to discern the two interaction points. To obviate, it should be introduced an effective photoelectric cross section $\sigma_{ph,eff}$. Moreover, numerical integration for the computed errors should be introduced, as the error on the cosine of the scattering angle widely depends on the distance between interaction points and the linear approximation is not viable in the most extreme cases. The program can be relatively easily multi-threaded, with performance increasing linearly as it is possible to assign an event to every core, without needing data sharing between the cores. At last, in some cases the same quantity is still computed more than once and a thought out process to avoid the issue could be implemented.

Part III

A PRELIMINARY EXPERIMENTAL TEST

This section contains a preliminary analysis of experimental data taken with AGATA and a ^{137}Cs source. The scope is to familiarize with the analysis procedure as well as ponder some of the challenges of the experiment. Some preliminary qualitative comparison between the experimental and simulated data will be carried out.

3

EXPERIMENTAL DATA FROM A ^{137}CS SOURCE

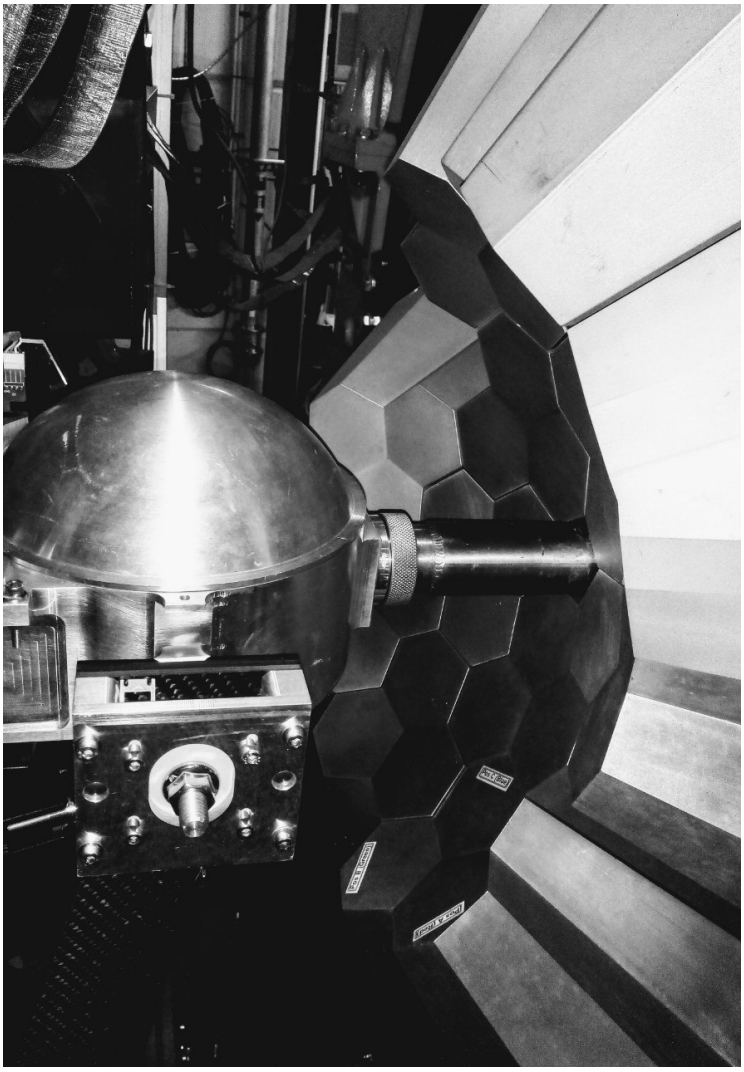

Figure 22: Photo of the AGATA tracking array at the time of the measurement. The source was placed at the nominal position inside the reaction chamber of aluminum. Facing the detector from the front, and not shown in this picture, NEDA [26], the neutron detector which makes use, among other, of lead shielding.

The following experimental data was taken at the GANIL laboratory in Caen, France, where AGATA is currently located. It was measured with a source of ^{137}Cs with an activity of 28.7 kBq. While the complete setup consisted in 12 triple crystals as shown in the simulation, crystal 09A was not operational at the time of the experiment. The overall performance was very satisfactory with few issues arising during the time span of the data taking.

The data was saved in the form of long traces, thus allowing multiple *replays* of the data preprocessing, pulse shape analysis and post-processing of the acquisition procedure. These allowed to tweak the configuration settings such as the cross talk matrices or the trapping parameters for some of the crystals. This choice proved crucial as some issues were solved by taking advantage of the mentioned features.

A *replay* consists in reproducing a part of choice of the signal analysis process. Through the *femul* emulator [27], it is possible to run a specific step (PSA, post PSA, event builder, tracking) on a specific crystal, on a group of crystals or on the full array. This feature proved very advantageous as the computational power needed to run a full replay is outside the reach of a common computer and would not allow to appreciate the tweaks made in the various procedures in a reasonable time frame. A full PSA *replay* was needed only for four crystals.

Additional data consisting on a ^{60}Co calibration and background runs of two days were taken. The high statistics acquired with ^{60}Co allowed the generation of the cross talk matrices on a problematic crystal, as well as the update of the trapping parameters [28] (required for the neutron damage correction) on another detector.

A complete electronics (digitizers) restart was needed after the calibration due to the presence of double peaks in the core signals of two detectors.

While Chapter 2 focused on a simple emission of single or double gamma, in reality the process is more complicated. Figure 23 shows the decay scheme of the mother isotope ^{137}Cs. This nucleus decays always via emission of a β^- particle, with a 94.7% branching on the $\frac{11}{2}^-$ state of 661.7 keV. The decay percentage on the lower lying level $\frac{1}{2}^+$ can be considered negligible and not much of a disturbance to the measurement (5.8×10^{-4}%).

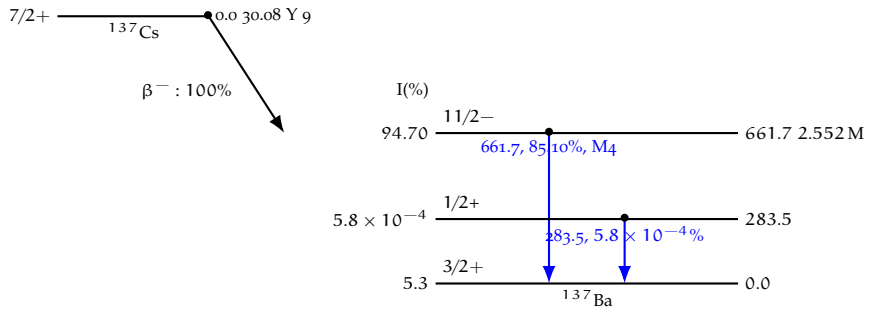

Figure 23: β^- decay scheme of ^{137}Cs. The $\frac{11}{2}^-$ state decays via a M4 transition to the $\frac{3}{2}^+$ ground state level.

Another experimental aspect of the decay are the X-rays emitted by the electrons of ^{137}Ba subsequent to the decay. Their energies range from 31.8 keV to 37.3 keV [29].

Moreover computing the number of single gammas which fully deposit their energy in the array returns an information of interest. Taking into account the difference in efficiency as well as the double gamma discard rate (Table 3), it is possible to estimate that for the observation of a total of 10000 double gamma events, 259.7 Tb of data are needed, if the full traces are saved. Only recording

the hits would greatly reduce the amount of data, while losing the possibility of further *replays*.

3.1 CALIBRATION OF THE ARRAY

Before analyzing the data produced by AGATA, a calibration of the array and other procedures are needed. The calibration consisted in aligning the energy spectra of 35 crystals each with 36 segments and a common core, for a total of 1260 independent spectra.

The calibration data was taken only with ^{60}Co. A calibration with this isotope on its own will not result in optimal outcomes at low energy, as the decay features two nearby peaks at 1332.5 keV and 1173.2 keV, resulting in low precision on the offset of the calibration. However, at the time of the measurement a ^{152}Eu source was not available.

After a first post-PSA calibration, the energy spectra were showing the aforementioned peak centroids well within 1 keV of each other, while low energy peaks were affected by unsatisfactory alignment (more than 3 keV on some segments). While this problem can be fixed by using the Europium source, an adequate, although not optimal, calibration was reached via a linear regression on the Gaussian fit of the two Cobalt peaks as well as the highest statistics Cesium data. Due to the higher statistics of the Cesium run, a weight on the regression point equal to the square root of the counts within the Gaussian was used. The regression was carried on via minimization of the weighted least squares, by solution of the normal equation $\theta = (X^T X)^{-1} X^T y$, where X is the matrix containing the fitted centroids multiplied by their weight and θ is the vector of the coefficients (offset and gain). An attempt to include the ^{40}K background peak at 1460.8 keV peak was made. This isotope is commonly present in nature and appears clearly in the measured spectrum. Fitting the peak, however, proved inconsistent results as some of the segments did not have enough counts for its correct detection. However, the peak lies close to the fitted ^{60}Co peaks and, when included was not showing benefits in the outcome of the calibration.

The *Force-Core-to-Segment* procedure, while in most cases is able to improve the spectrum by using the core signals, in others had to be disabled on a specific crystal. In fact, when a segment was affected by a resolution considerably higher than the other, the *Force-Core-to-Segment* procedure was introducing some artifacts. A hit that is registered at higher energy in the affected segment due to the high peak width, tricks the procedure into redistributing more of the core energy to the segment itself, while lowering the energy given to all other segments, thus creating a left tail on all the peaks of the crystal. This effect can be destructive for the tracking and to avoid artifacts or unwanted results, the procedure was disabled on the problematic crystals and the output of the segment showing unsatisfactory resolution was discarded. Segments (sgm.) affected by this issue were sgm. 5 of crystal 02C and sgm. 5 of crystal 06C.

In other cases (00A, 01B, 11A and 14C), a choice to eliminate a segment affected by low resolution at the pre-processing level and generate its signal from the cross

talk matrix was made. This is possible only if all other segments are performing well.

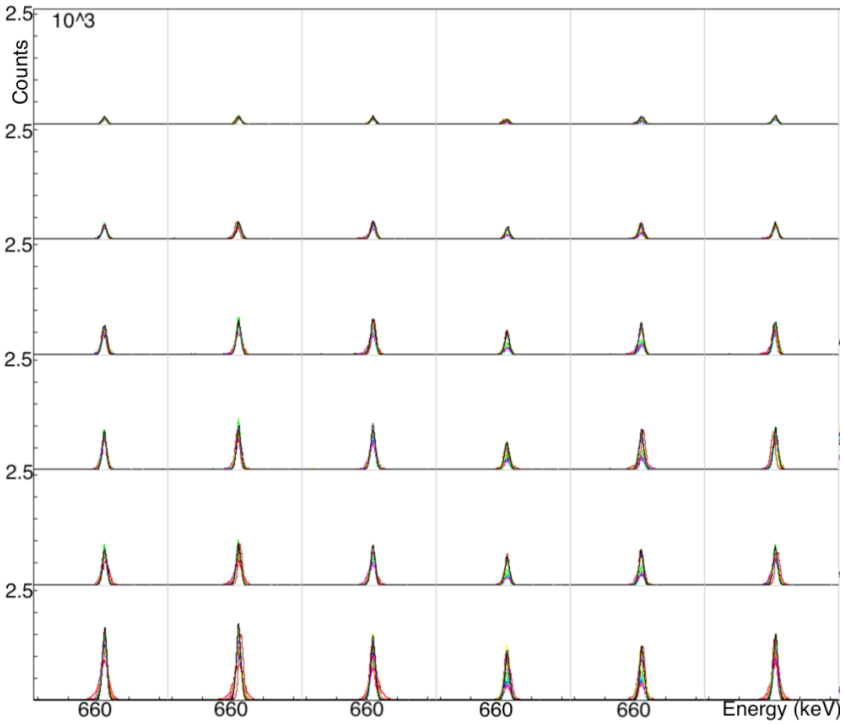

Figure 24: Matrix of spectra relative to the ^{137}Cs 661.7 keV peak after calibration and neutron damage correction in every segment of all crystals A of every triple cluster. The last column from the right represents the core signals at different gains and the sum of the segment spectra.

3.2 CHALLENGES OF THE MEASUREMENT

3.2.1 *PSA clustering*

The hit position as a function of the emission angle is expected to show a uniform distribution for a single gamma emission from a source. The interaction hits in the crystal should be uniform on the plane equidistant from the source while in the depth dimension, the number of interactions should decay exponentially starting from the maximum located on the surface. The exponential attenuation coefficient depends on the numeric density of scattering centers in the crystals (electrons) and on the cross section of the interaction process.

Figure 25 shows three cross sections of a single crystal:

- A longitudinal cross section (b): most hits are registered in the first cm of Germanium. However, the maximum number of counts does not occur at the surface (located at 0 mm), but slightly after, around 5 mm. The PSA struggles at recognizing hits on the limiting surface of the segment, the same effect is visible deeper in the crystals, where the individual segments are clearly distinguished by contours generated by a lower number of hits.

- A cross section parallel to the detector front-face at a distance of 18 mm (c) and 74 mm (d): interaction points are clustered in some regions while other show fewer counts. This effect is observed in all depths of the crystal.

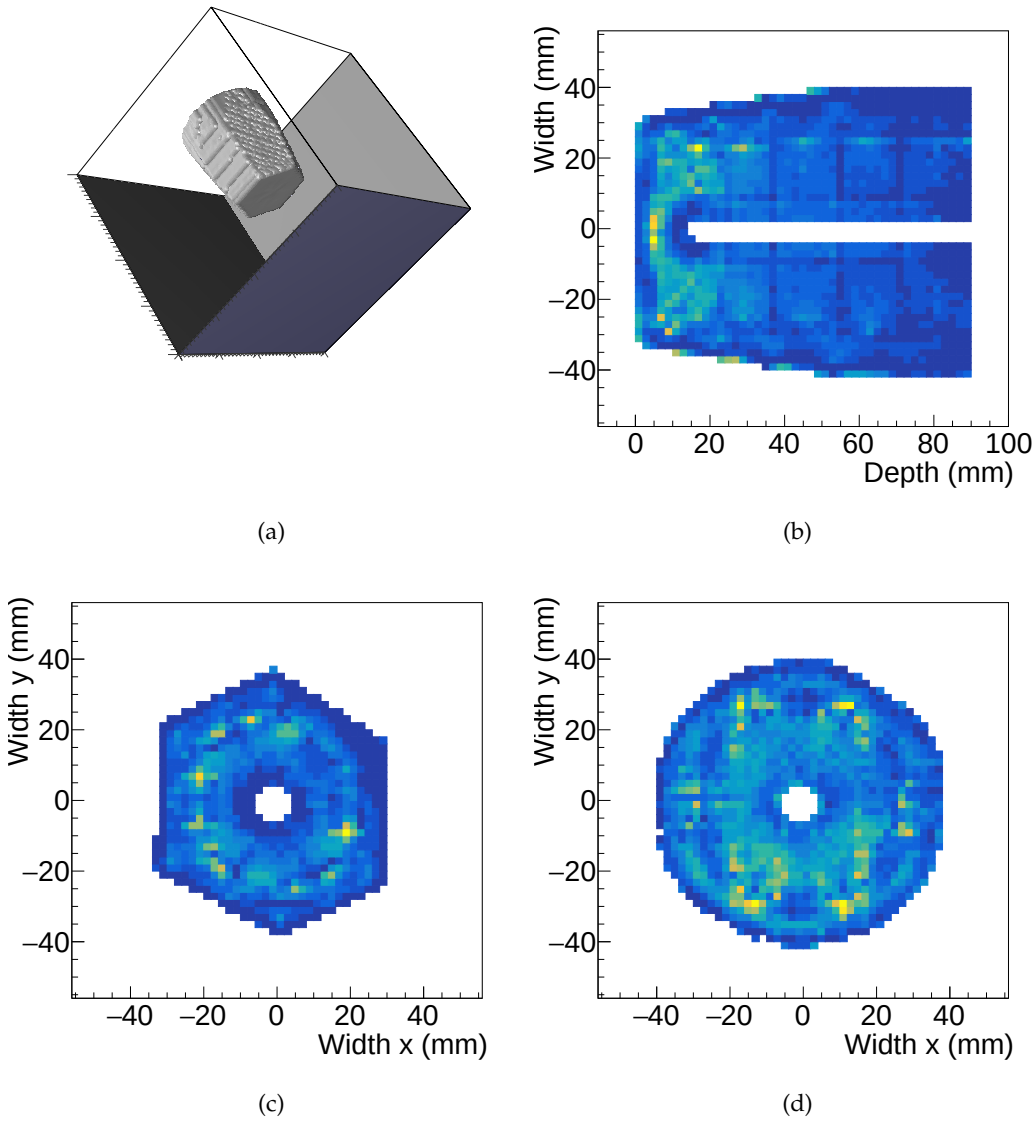

Figure 25: Examples of PSA clustering in one AGATA crystal (02B) with the ^{137}Cs source. The binning corresponds to the position resolution of the PSA. (a) is a plot of the sum of all interactions in the crystal and shows the shape of the HPGe crystal. (b) shows the interaction points in the longitudinal cross-section of the same crystal, while (b) and (c) represent the cross-section at two different depths, 18 mm and 74 mm from the surface, respectively.

This phenomenon poses a challenge for the tracking, which relies on an unbiased measurement of the gamma interaction position to compute the merit factors. This bias, in theory, could introduce systematic errors in the tracking event

reconstructions, and more precise quantization should be performed to asses its entity.

Some crystals are affected more than others by the issue and the particular example shown in Figure 25, 02B, was showing one of the most not-uniform distributions.

3.2.2 *Stability of the system*

Due to the rarity of the decay, the measurement is expected to span over multiple days or months. Thus the overall stability of the array is a crucial aspect to take into account. During the data taking session presented in this thesis, no significant issues were found, aside from the regular resetting, from the run control, of the unlinked optical links of some crystals.

The energy spectra could, in theory, fluctuate over time due to changes on the environmental condition of the crystals or issues related to the electronics stability. This might be destructive for a good outcome of the tracking, as a particular precision on the energy calibration is necessary. To test this aspect it is possible to plot the energy deposited in every hit as a function of time; if the spectral lines remain stable during the course of the experiment, the issue can be disregarded. The measurement was performed during over 45 hours and a negligible variation of less than 0.5 keV was observed, as a consequence Figure 26 shows the single segment spectrum over time, namely crystal 11B, segment 6. Once again no fluctuations can be observed.

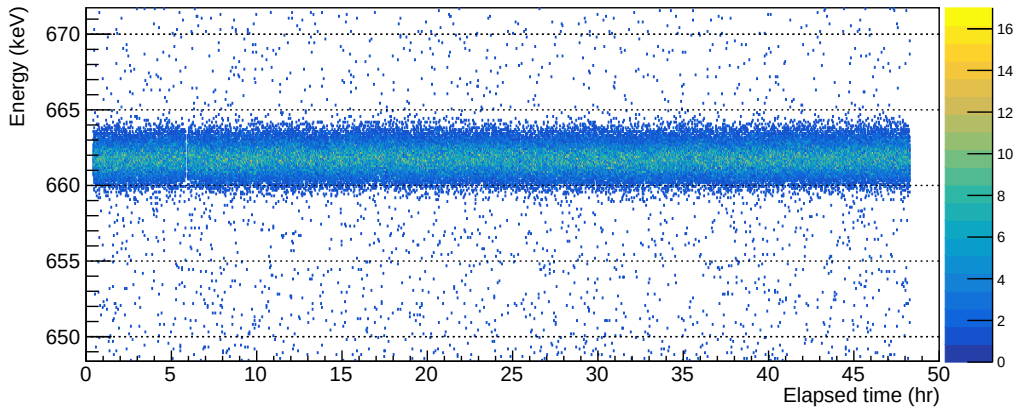

Figure 26: Spectrum of the deposited energy in a single segment (6 of crystal 11B) as a function of time. The segment remained remarkably stable in the time span of the acquisition, with no fluctuations evident, even during the filling of the dewars with liquid nitrogen.

3.2.3 *Neutron damage corrections*

Every detector subject to in beam experiments can experience a high flux of energetic neutrons. These particles, due to their neutral charge, are able to penetrate

deeply in the Germanium crystals and damage their crystalline structure creating traps for the electrons that have the consequence of lowering the energy resolution of the detector.

The effect is quite evident in spectral peaks (Figure 27) as the impurities in the structure can cause a lower amount of collected charge, leaving a significant left tail in the pick.

The issue can be corrected, as described in reference [28] and is able to improve dramatically the resolution of the affected peaks.

The procedure consists in evaluating the trapping sensitivity, a quantity dependent on the collection efficiencies of the charge carriers, as a function of the detector volume during the PSA. The trapping sensitivity is then used to correct segment by segment the hit energy and the original energy resolution can be optimally recovered up to a certain quantifiable limit of degradation due to statistical fluctuations caused by trapping effects.

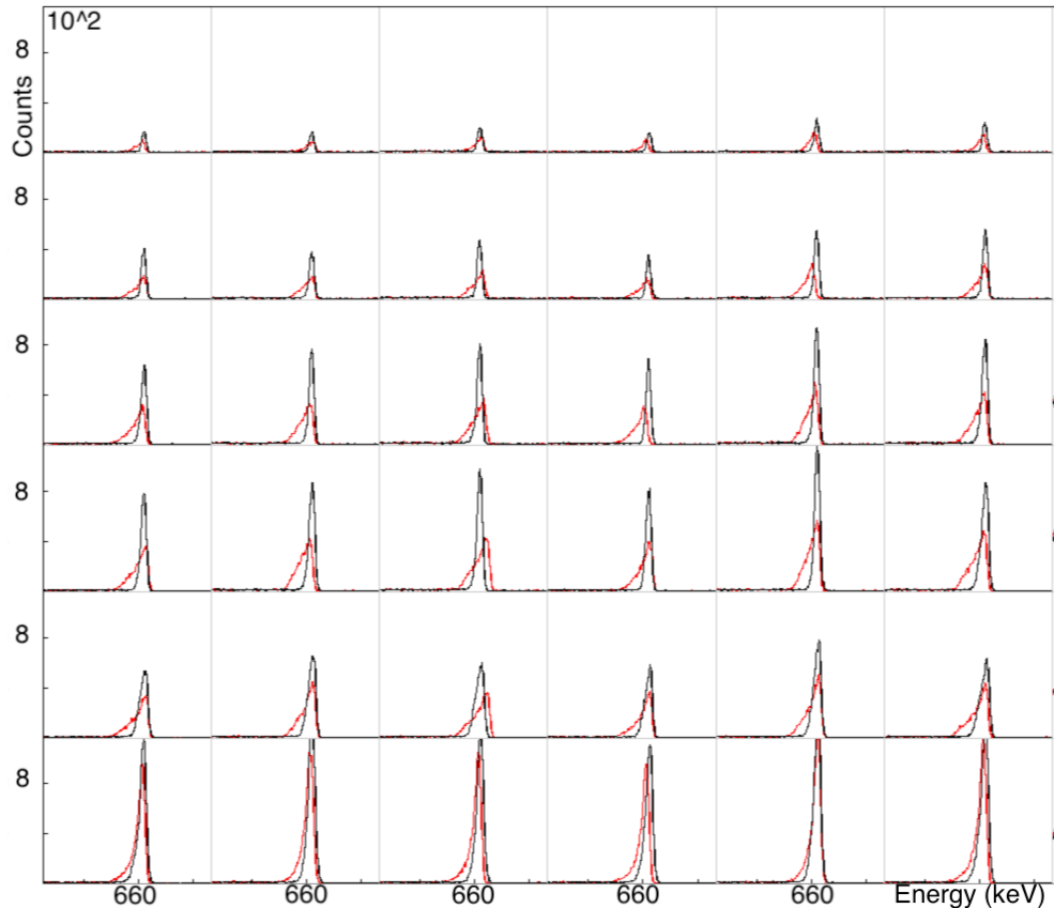

Figure 27: 10B crystal before (red) and after (black) the neutron damage correction. Every panel in the matrix represents a single segment.

In the case of this data acquisition session, the trapping coefficients of one crystal had to be generated as the neutron damage procedure was overcompensating the correction and generating right tails in some peaks. This procedure was able

to improve the resolution by a factor of up to 2 in the peaks most affected by the issue.

3.2.4 *Background radiation*

Background radiation is a very important aspect to take into account for the double-gamma decay measurement that is characterized by such a low branching ratio. Figure 29 shows the gamma spectrum obtained during the measurement with the ^{137}Cs source. Many contaminants are present and the most prominent peaks are labeled. One can observe ^{40}K as well the radiation caused by nuclei in the decay chain of ^{232}Th (such as ^{208}Tl and ^{228}Ac) and those from ^{238}U or ^{234}U (such as ^{214}Bi).

Figure 30, on the other hand, shows the fold two coincidences in the region of interest. Diagonal lines correspond to Compton scattered photons not fully reconstructed while vertical or horizontal lines represent a coincidence of a completely tracked gamma with a photon which has not fully deposited its energy in the array.

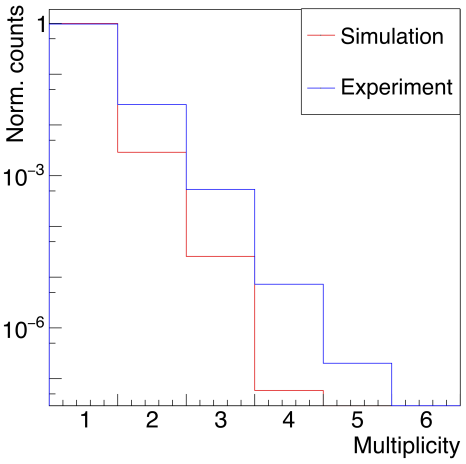

Figure 28: Normalized histogram of gamma multiplicity for the experimental data and the simulation, obtained with the same tracking parameters.

Figure 28 shows multiplicity of the tracked gammas without any conditions applied in the simulation and in the experiment when the same tracking parameters were set.

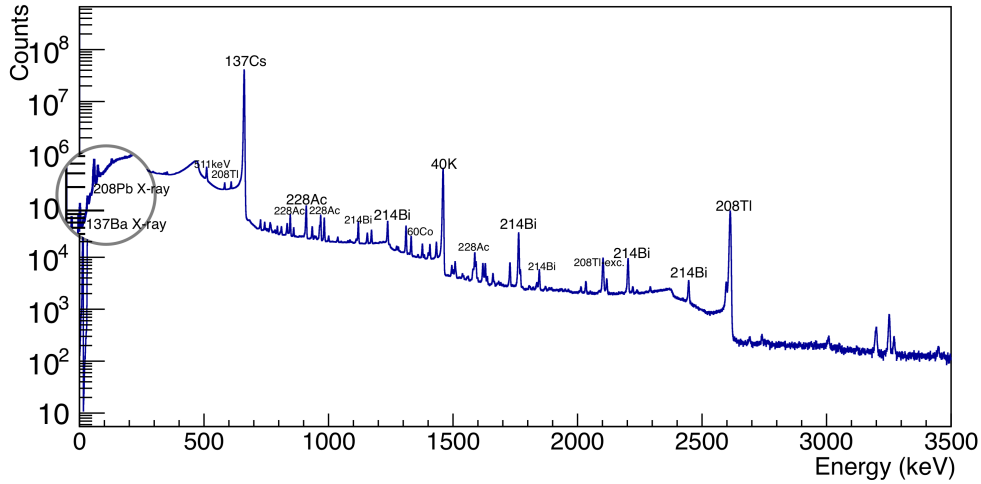

Figure 29: Gamma-ray energy spectrum taken during this measurement with the ^{137}Cs source. The enhanced low energy portion shows the X-rays of ^{137}Ba (36.3 keV) subsequent to the β^- decay of ^{137}Cs and of ^{208}Pb (75.0 keV) which is observable due to the presence of lead shielding in the nearby NEDA array [30, 31]. The lower and more intense ^{137}Ba X-ray emission at 32.2 keV is not observed due to the fact that the electronics threshold was set higher.

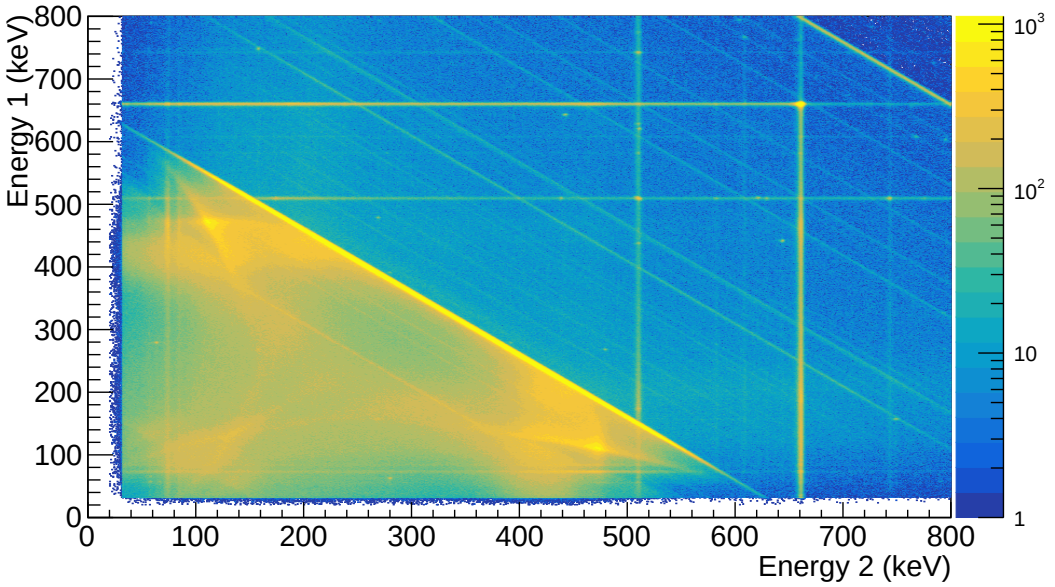

Figure 30: Gamma-gamma coincidence matrix for two tracked gammas. In the region of interest, the matrix shows the expected simultaneous observation of two 661.7 keV gammas as well as the 511 keV peak (pair production peak of higher energy background gammas). Other interesting features are the Compton edges (477.3 keV) in coincidence with the lower end of the Compton distribution.

3.3 HOW DOES THE SIMULATION COMPARE

The most interesting aspect of a first experimental approach is to compare the experimental results with the ones obtained in the simulation. Using the parameters found in Section 2.2, it is possible to operate a direct comparison. The data here presented has been selected with the same conditions of the simulation (Section 2.5) and with an additional condition on the time difference on the tracked gammas inferior to 5 ns.

The experimental 2D plots shown in Figure 31 present similar features to Figures 16, 18 and 19 (a) (which correspond to the simulation of a single gamma event).

While the same configurations are evident, Figure 31 (b) presents a distribution of events corresponding to Compton scattered photons. In the simulation, however, the tracking parameters were showing promising results in that regard, as no peak was seen in correspondence to the red line (equation 1) after the optimization. Further investigation is needed to understand what is causing this issue.

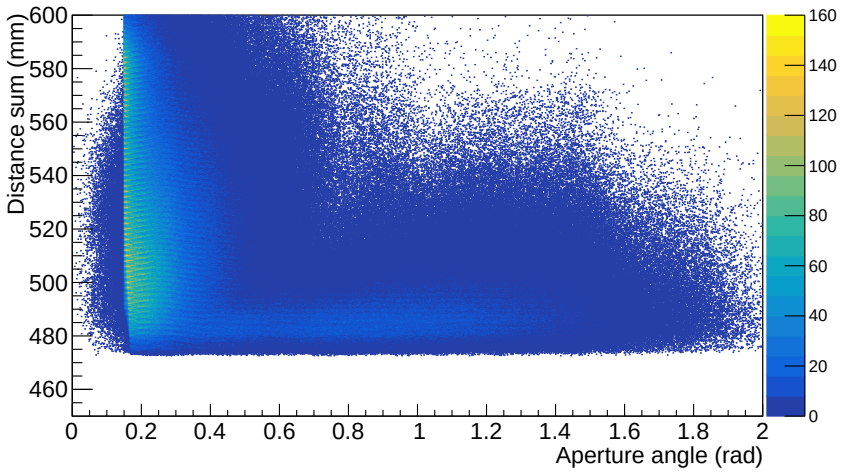

(a)

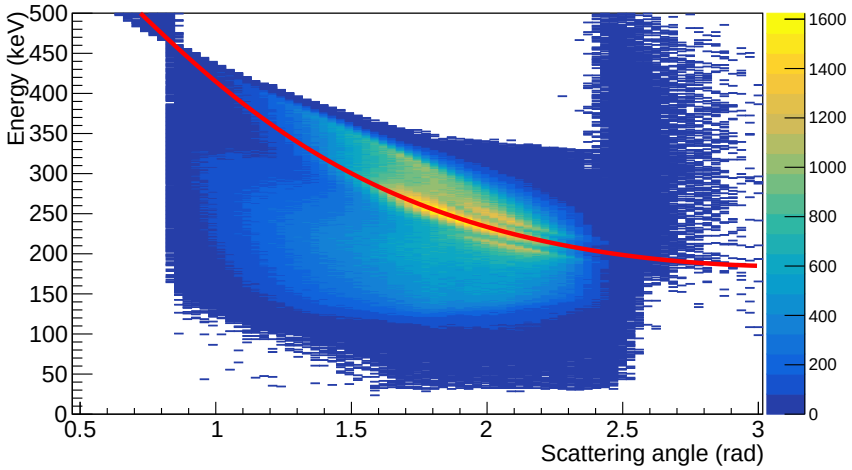

(b)

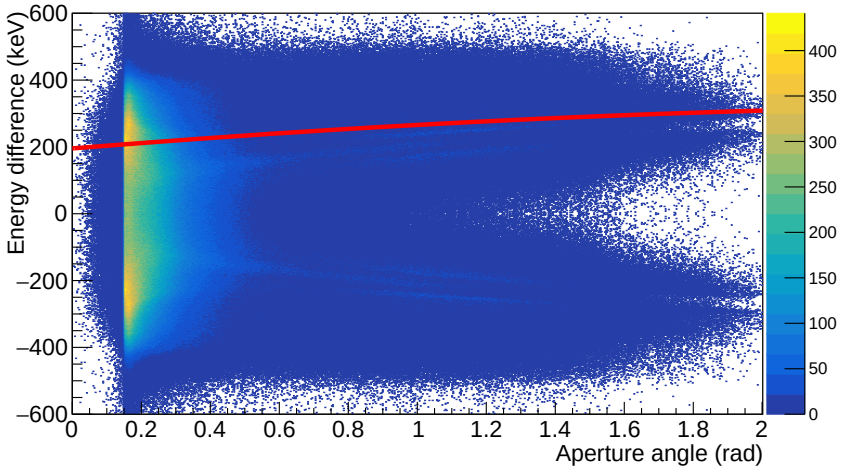

(c)

Figure 31: Experimental data relative to: (a) Figure 16, (b) Figure 18 and (c) Figure 19. Scattering photons have been reconstructed with the same tracking parameters as the simulation (Table 2). The red lines in (b) and (c) correspond to what has been described in Section (2.5).

4

CONCLUSIONS AND FURTHER PERSPECTIVES

In this thesis the capability of AGATA to measure the rare competitive double-gamma decay has been studied with a detailed simulation. This consists in a rare process, in which an excited state of a nucleus decays emitting two gamma rays despite the emission of a single photon is allowed. From a theoretical standpoint, the decay is correctly described as a second order process in perturbative QED.

The measurement, would not only return more detailed physical information, namely on the energy and angular distributions of the photons, but also test the capabilities of the advanced gamma-ray spectrometer AGATA. The main challenge that the measurement faces is the suppression of Compton events without relying on timing properties due to the resolution limitations of germanium detectors. The thesis is focused on assessing whether the good energy resolution and spatial reconstruction properties of the detector, together with a strict event selection and optimization, are able to overcome the difficulties of such measurement.

The emission of single and double-gamma photons has been simulated and optimal values of the algorithms were found for this specific measurement. The performance of the tracking was characterized and a further event selection was performed. While the measurement of the competitive double-gamma decay has proved itself challenging from an experimental standpoint, the current work only represents a starting point and a statement of the current capabilities. In fact, while the tracking algorithm showed a good performance with its optimal parameters (Table 3), the need for a specific algorithm is argued in this thesis. In that sense, the community is also working towards new tracking algorithms based on a different statistical approach [23, 24]. Since the array is in continuous development and improvement by the AGATA community, many progresses are expected as the research proceeds and many of them will likely be of crucial importance for the measurement of the competitive double-gamma decay. At last, a preliminary analysis of data taking with AGATA and a ^{137}Cs source was performed. The background activity as well as the neutron damage correction and the stability of the calibration over time during the time span of the experiment have been discussed. While the analysis is only preliminary, a final comparison between the experimental data and the simulation has been performed.

Increasing the experimental position resolution, as well being able to recognize multiple hits within the same segment could be crucial for future measurements. This aspects can be tested with a simulation by modifying the packing volume, which consists in the minimum resolvable distance between two different interaction points. This aspect is of great importance especially for low-energy photons.

More refined statistical analysis of the process could greatly improve the performance of the tracking, and improvements can be made in that regard.

At last, a future increase of the solid angle coverage of the AGATA array will improve the sensitivity of the double-gamma detection, opening new possibilities for the measurement of lower branching ratio double-gamma decays.

BIBLIOGRAPHY

[1] J. Kramp, D. Habs, R. Kroth, M. Music, J. Schirmer, D. Schwalm, and C. Broude. "Nuclear two-photon decay in 0+->0+ transitions." In: *Nuclear Physics A* 474.2 (1987), pp. 412 –450. ISSN: 0375-9474.

[2] E. Beardsworth, R. Hensler, J. W. Tape, N. Benczer-Koller, W. Darcey, and Jack R. MacDonald. "Double Gamma Decay in ^{40}Ca." In: *Phys. Rev. C* 8 (1 1973), pp. 216–229.

[3] C. Walz, H. Scheit, N. Pietralla, T. Aumann, R. Lefol, and V. Yu Ponomarev. "Observation of the competitive double-gamma nuclear decay." In: *Nature* 526 (2015), 406 EP.

[4] E. Merchán, K. Moran, C.J. Lister, P. Chowdhury, E.A. McCutchan, J.P. Greene, S. Zhu, T. Lauritsen, M.P. Carpenter, and R. Shearman. "^{137}Ba Double Gamma Decay Measurement with GAMMASPHERE." In: *EPJ Web of Conferences* 93 (2015), p. 01033.

[5] J. Engel and J. Menéndez. "Status and future of nuclear matrix elements for neutrinoless double-beta decay: a review." In: *Reports on Progress in Physics* 80.4 (Apr. 2017), p. 046301.

[6] J. Menendez et al. In: *Private communication* (2018).

[7] D.P. Grechukhin. "Model estimates of the probability for two-quantum transitions of nuclei (III)." In: *Nuclear Physics* 62.2 (1965), pp. 273 –295. ISSN: 0029-5582.

[8] J. L. Friar. "Low-energy theorems for nuclear Compton and Raman scattering and $0^+ \to 0^+$ two-photon decays in nuclei." In: 201 (1975), pp. 170–201.

[9] C. Walz. "The two-photon decay of the $\frac{11}{2}^-$ isomer of ^{137}Ba and mixed-symmetry states of ^{92,94}Zr and ^{94}Mo." In: *PhD dissertation, Technischen Universität Darmstadt* (2014).

[10] G.F. Knoll. *Radiation detection and measurement*. Wiley, 1989.

[11] S.M. Seltzer J. Chang J.S. Coursey R. Suku-mar D.S. Zucker M.J. Berger J.H. Hubbell and K. Olsen. "XCOM: Photon Cross Sections Database." In: *National Institute of Standards and Technology* (2018). URL: http://www.nist.gov/pml/data/xcom/,2014..

[12] S. Akkoyun et al. "AGATA - Advanced GAmma Tracking Array." In: *Nuclear Instruments and Methods in Physics Research, Section A: Accelerators, Spectrometers, Detectors and Associated Equipment* 668 (2012), pp. 26–58. ISSN: 01689002. DOI: 10.1016/j.nima.2011.11.081. arXiv: 1111.5731.

[13] E. Farnea, F. Recchia, D. Bazzacco, Th. Kröll, Zs. Podolyak, B. Quintana, and A. Gadea. "Conceptual design and Monte Carlo simulations of the AGATA array." In: *Nuclear Instruments and Methods in Physics Research Section A: Accelerators, Spectrometers, Detectors and Associated Equipment* 621.1 (2010), pp. 331 –343. ISSN: 0168-9002.

[14] A. Wiens, H. Hess, B. Birkenbach, B. Bruyneel, J.Eberth, D. Lersch, G. Pascovici, P. Reiter, and H. Thomas. "The AGATA triple cluster detector." In: *Nuclear Instruments and Methods in Physics Research Section A: Accelerators, Spectrometers, Detectors and Associated Equipment* 618.1 (2010), pp. 223 –233. ISSN: 0168-9002.

[15] P.-A. Söderström et al. "Interaction position resolution simulations and in-beam measurements of the AGATA HPGe detectors." In: *Nuclear Instruments and Methods in Physics Research Section A: Accelerators, Spectrometers, Detectors and Associated Equipment* 638.1 (2011), pp. 96 –109. ISSN: 0168-9002.

[16] D. Bazzacco R. Venturelli. "Adaptive grid search as pulse shape analysis algorithm for gamma-tracking and results." In: *LNL Annual Report* (2004).

[17] I. Abt, A. Caldwell, D. Lenz, J. Liu, X. Liu, and B. Majorovits. "Pulse shape simulation for segmented true-coaxial HPGe detectors." In: *European Physical Journal C* 68.3 (2010), pp. 609–618. ISSN: 14346044.

[18] Th. Kröll et al. "In-beam experiment with the γ-ray tracking detector MARS." In: *Nuclear Instruments and Methods in Physics Research Section A: Accelerators, Spectrometers, Detectors and Associated Equipment* 586.3 (2008), pp. 421 –431. ISSN: 0168-9002.

[19] B. Birkenbach. "Gamma ray tracking with the AGATA demonstrator: A novel approach for in-beam spectroscopy." In: (2014).

[20] A. Lopez-Martens, K Hauschild, A Korichi, J Roccaz, and J. P. Thibaud. "Gamma-ray tracking algorithms: A comparison." In: *Nuclear Instruments and Methods in Physics Research, Section A: Accelerators, Spectrometers, Detectors and Associated Equipment* 533.3 (2004), pp. 454–466. ISSN: 01689002.

[21] D. Bazzacco. "The Advanced Gamma Ray Tracking Array AGATA." In: *Nuclear Physics A* 746 (2004). Proceedings of the Sixth International Conference on Radioactive Nuclear Beams (RNB6), pp. 248 –254. ISSN: 0375-9474.

[22] S. J. Colosimo. "The Characterisation of AGATA High Purity Germanium Detectors for Pulse Shape Analysis." In: *PhD Thesis* (2013).

[23] H. Egger M. Reese N. Pietralla P. Napiralla C. Stahl. "Bayes-Tracking – A new Approach for Gamma Ray Tracking." In: (2017). URL: https://indico.in2p3.fr/event/13409/contributions/14183/subcontributions/571/attachments/11820/14546/Bayes-Tracking.pdf.

[24] P. Napiralla et al. "Bayes-Tracking – A new Approach for Gamma Ray Tracking." In: *Nuclear Instruments and Methods in Physics Research, to be submitted* (2018).

[25] D. Brugnara. In: *GitHub* (2018). URL: https://github.com/danielebrugnara/Trackingdouble/tree/correct-energies.

[26] T. Hüyük. "The Next Generation Nuclear Instruments: AGATA and NEDA, and Nuclear Structure Studies near N=Z line." In: *PhD Thesis* (2017).

[27] O. Stézowski. "AGATA Data Analysis for the GANIL Phase." In: *AGATA Week, GANIL* (2014). URL: http://pro.ganil-spiral2.eu/events/workshops/previous/agataws/agata-week-2014/presentations/3-data-analysis/stezowski_dataanalysis.pdf/at_download/file..

[28] The AGATA Collaboration et al. "Correction for hole trapping in AGATA detectors using pulse shape analysis." In: *The European Physical Journal A* 49.5 (2013), p. 61. ISSN: 1434-601X.

[29] In: *National Nuclear Data Center, Brookhaven National Laboratory* (2018). URL: http://www.nndc.bnl.gov/chart/decaysearchdirect.jsp?nuc=137CS&unc=nds.

[30] J.J. Valiente-Dobón et al. "NEutron Detector Array: NEDA." In: *Nuclear Instruments and Methods in Physics Research, to be submitted* (2018).

[31] T. Huyuk et al. "Conceptual design of the early implementation of the NEutron Detector Array (NEDA) with AGATA." In: *European Physical Journal A* 52.3 (2016), pp. 55–9.